A HETERODYNE DETECTION FM-CW LASER RADAR USING A 10.6 μ SOURCE

Maurice F. Fraunfelder

NAVAL POSTGRADUATE SCHOOL
Monterey, California

THESIS

A HETERODYNE DETECTION FM-CW

LASER RADAR USING A 10.6 μ SOURCE

by

Maurice F. Fraunfelder, Jr.

December 1974

Thesis Advisor: T. F. Tao

UNCLASSIFIED

SECURITY CLASSIFICATION OF THIS PAGE (When Data Entered)

REPORT DOCUMENTATION PAGE		READ INSTRUCTIONS BEFORE COMPLETING FORM
1. REPORT NUMBER	2. GOVT ACCESSION NO.	3. RECIPIENT'S CATALOG NUMBER
4. TITLE (and Subtitle) A Heterodyne Detection FM-CW Laser Radar Using a 10.6 μ Source		5. TYPE OF REPORT & PERIOD COVERED Electrical Engineer Thesis; December 1974 6. PERFORMING ORG. REPORT NUMBER
7. AUTHOR(s) Maurice F. Fraunfelder, Jr.		8. CONTRACT OR GRANT NUMBER(s)
9. PERFORMING ORGANIZATION NAME AND ADDRESS Naval Postgraduate School Monterey, California 93940		10. PROGRAM ELEMENT, PROJECT, TASK AREA & WORK UNIT NUMBERS
11. CONTROLLING OFFICE NAME AND ADDRESS Naval Postgraduate School Monterey, California 93940		12. REPORT DATE December 1974 13. NUMBER OF PAGES 114
14. MONITORING AGENCY NAME & ADDRESS (if different from Controlling Office) Naval Postgraduate School Monterey, California 93940		15. SECURITY CLASS. (of this report) Unclassified 15a. DECLASSIFICATION/DOWNGRADING SCHEDULE

16. DISTRIBUTION STATEMENT (of this Report)

Approved for public release; distribution unlimited.

17. DISTRIBUTION STATEMENT (of the abstract entered in Block 20, if different from Report)

18. SUPPLEMENTARY NOTES

19. KEY WORDS (Continue on reverse side if necessary and identify by block number)

Lidar
Optical radar
FM-CW radar
Range and velocity measurement
Acousto-optic modulation

20. ABSTRACT (Continue on reverse side if necessary and identify by block number)

The feasibility of a heterodyne detection FM-CW laser radar capable of providing simultaneous range and velocity information was investigated. Linear triangular frequency modulation was accomplished with an acoustooptic modulator. Two separate optical configurations were investigated. Ranges to 2400 ± 30 yards were measured using a two-inch retro-reflector as a target, with a 7000-yard maximum predicted

DD FORM 1 JAN 73 1473 (Page 1)

EDITION OF 1 NOV 65 IS OBSOLETE
S/N 0102-014-6601

UNCLASSIFIED

SECURITY CLASSIFICATION OF THIS PAGE (When Data Entered)

range. Velocities as low as .37 m/sec were easily measured, and the system was estimated to have a velocity resolution of approximately .05 m/sec. The measured receiver sensitivity was approximately 30 db below the theoretical limit. Possible causes and remedies for this reduced sensitivity are presented. An unexplained zero velocity return was observed from a moving target with the second optical configuration. A signal contamination of the local oscillator beam was also observed. Investigations of the cause of this contamination and possible explanations are presented.

Simultaneous results of this project are reported in FM-CW Laser Radar at 10.6 Microns, a thesis by Lieutenant T.H. Chance [Ref. 7].

A Heterodyne Detection FM-CW Laser Radar Using a 10.6 μ Source

by

Maurice F. Fraunfelder, Jr.
Lieutenant, United States Navy
B.S.E.E., Purdue University, 1969
M.S.E.E., Naval Postgraduate School, 1974

Submitted in partial fulfillment of the
requirements for the degree of

ELECTRICAL ENGINEER

from the

NAVAL POSTGRADUATE SCHOOL
December 1974

ABSTRACT

The feasibility of a heterodyne detection FM-CW laser radar capable of providing simultaneous range and velocity information was investigated. Linear triangular frequency modulation was accomplished with an acoustooptic modulator. Two separate optical configurations were investigated. Ranges to 2400 ± 30 yards were measured using a two-inch retro-reflector as a target, with a 7000-yard maximum predicted range. Velocities as low as .37 m/sec were easily measured, and the system was estimated to have a velocity resolution of approximately .05 m/sec. The measured receiver sensitivity was approximately 30 db below the theoretical limit. Possible causes and remedies for this reduced sensitivity are presented. An unexplained zero velocity return was observed from a moving target with the second optical configuration. A signal contamination of the local oscillator beam was also observed. Investigations of the cause of this contamination and possible explanations are presented.

Simultaneous results of this project are reported in FM-CW Laser Radar at 10.6 Microns, a thesis by Lieutenant T. H. Chance [Ref. 7].

TABLE OF CONTENTS

LIST OF FIGURES

ACKNOWLEDGEMENTS

I wish to express sincere appreciation to the Naval Electronics Laboratory Center San Diego, Code 2500, particularly to Dr. Greg Mooradian and Rudy Krautwald. Without their advice and equipment support, this project would not have been possible. I am additionally grateful for the assistance of Professors John Powers and T. F. Tao of the Naval Postgraduate School.

I wish to thank Dr. J. Longo of the Rockwell International Science Center and Dr. Peter Wang of Aerojet General Corporation for the loan of state of the art detectors which were used or evaluated in this project.

Lastly I would like to thank my co-worker and academic colleague Lieutenant Thomas H. Chance, with whom this joint project was conducted.

I. INTRODUCTION

One of the primary advantages of a laser communications or radar system is the enormous economically achievable antenna gain and hence excellent spatial resolution. Another advantage is the extreme receiver sensitivity if shot noise limited operation is achieved with a heterodyne detection system [Refs. 1, 2, 3, and 4]. Several communications and radar systems have been built that approach within an order of magnitude the theoretical quantum or shot noise limit [Ref. 5].

The combinations of the well known 8-13 micron atmospheric window; high available output powers; high conversion efficiencies; and detectors with high quantum efficiencies indicate that a carbon dioxide wavelength system may be the best candidate for an optical radar [Ref. 5].

Coherent (heterodyne) detection is more advantageous at longer optical wavelengths due to reduced quantum noise, less stringent optical alignment requirements, less atmospheric coherence degradation effects, and a larger resulting field of view for a fixed receiver aperture. Thus a longer wavelength system is capable of a greater sensitivity for a fixed field of view [Ref. 6].

In addition to the greater achievable sensitivity of heterodyne detection, it also offers considerably reduced background radiation interference and spatial signal

discrimination. The latter two combine to form a certain degree of immunity to jamming from hostile sources. Heterodyne detection also preserves the phase information contained within the transmitted signal. This allows the application of powerful signal processing techniques to extract maximum information from the returned signal.

A frequency modulated continuous-wave radar system has several advantages over the more conventional pulsed type radars. It has no minimum range; the range resolution is potentially greater than for pulsed systems; and it is less susceptible to narrow band jamming. The radar sensitivity is a function of the average output power, and for a continuous wave system this is the full laser power. In a pulsed system the average power is the laser power reduced by the duty cycle. The inherent coherent property of a continuous wave system allows for simultaneous measurement of both velocity and range information. Since the doppler information is proportional to the transmitted frequency, the extremely high frequency of an optical system should allow velocity measurements to a fraction of a meter per second.

The excellent angular resolution of the laser coupled with the excellent range resolution and high average powers of the continuous wave radar in conjunction with the ease and accuracy of velocity measurements indicate that a heterodyne detection, FM-CW laser radar may be a potentially useful system capable of development with current technology.

II. GENERAL THEORY OF OPTICAL DETECTION

Photo detectors fall into two classes: photon or quantum detectors and thermal detectors. The latter type are extremely narrow bandwidth low-pass devices and hence are inappropriate for communications or radar detector applications. Photon detectors can further be broken down into four basic types of detectors: photoemissive, photoconductor, photovoltaic, and photoelectromagnetic. Since photoemissive devices do not extent to wavelengths much greater than 1 μ [Refs. 3, 4, 8, and 9], and since the cumbersome magnetic field requirements and limited bandwidths of the photoelectromagnetic have limited its practical application, only photoconductor and photovoltaic devices will be discussed.

A. DETECTION MECHANISM IN SEMICONDUCTORS

For a photon to be absorbed by a semiconductor, it is necessary that the photon energy be greater than the material energy gap, E_g. This places a long wavelength limit, λ_c, on the photogeneration process given by

$$\lambda_c = \frac{h\nu}{E_g} .$$

The short wavelength limit is determined by carrier absorption at the semiconductor surface through surface trapping and absorption effects [Refs. 4, 9, and 10]. The detection

mechanism is a creation of excess charge carriers caused by the absorbed photon.

1. Photoconductors

This is the simplest type of detector. It consists of a single crystal slab of semiconductor material or of a thin film of semiconductor material deposited on a substrate. The thin film may be either single crystal or polycrystalline depending upon the material used. The detector is biased with an external potential as shown in Figure 12. The incident radiation changes the carrier concentration and hence detector conductivity, and the resulting change in detector current develops a potential signal across the load resistor. The signal current can be expressed by the following [Ref. 4].

$$i_s = \frac{\eta q}{h\nu} \left(\frac{\tau}{T}\right) \frac{1}{1 + (\omega_m \tau)^2} \frac{P_s}{2} [1 + m(t) \cos\omega_m t] \qquad (1)$$

where τ is the carrier lifetime, and T is the carrier transit time. From this it can be seen that the bandwidth of a photoconductor detector is carrier lifetime limited.

Extrinsic infrared photoconductors rely upon optical excitation of energy sites within the host crystal band gap. These energy sites are caused by impurities such as copper, mercury, cadmium or zinc. The prime disadvantage of this type of detector is the low temperature operating requirements [Refs. 3 and 9].

Intrinsic photoconductors utilize band-to-band excitation for the detection mechanism. Recent developments have been achieved with such mixed crystals as $Hg_{1-x}CD_xTe$ and $Pb_{1-x}Sn_xTe$ [Refs. 11, 12, 13, and 14]. The operating wavelength of these detectors can be controlled by varying the molar content x. The significance of these detector materials is a higher permissible operating temperature.

2. Photovoltaic or Photodiode Detectors

A photovoltaic detector consists of a p-n junction formed within an intrinsic semiconductor. Incident photons create an electron hole pair within the crystal bulk. If this carrier pair is generated within the depletion region or within a diffusion length of the depletion region, the internal electronic field of the diode will separate the charge carriers and a potential will be developed across the diode terminals. The photovoltaic detector's frequency response is a function of the carrier diffusion time, drift time within the depletion region, and junction resistance-capacitance.

However, measurement by Peyton and others [Ref. 2] on 2.5 μm HgCdTe photovoltaic detectors showed that the frequency response was limited by the RC constant of the p-n junction. Burke and Koehler have performed measurements on HgCdTe photodiodes at an elevated temperature of 170°K. A bandwidth of 200 MHz was achieved at 10.6 μm with 1.7 volt reverse bias [Ref. 15]. The technical importance of these measurements lies in satisfying the cooling requirement

with thermoelectric coolers. In general, photovoltaic detectors exhibit the highest detectivity when they are operated in the short-circuit or zero bias mode. For moderate or wide band operation, however, a reverse bias is usually applied to increase the bandwidth by decreasing junction capacitance.

B. SENSITIVITY COMPARISON OF OPTICAL HETERODYNE AND ENVELOPE (DIRECT) DETECTION

1. Envelope Detection Sensitivity

Photodetectors convert the absorbed optical radiation into electrical output signals. They are square law devices that respond to the intensity of light averaged over a few optical cycles. This is due to the limited speed of response of the carrier transport and relaxation processes within the detector. These responses do not have sufficiently short time constants to respond to the optical field variations. The expression for the conversion of the incoming optical power into a direct current is:

$$I_s = \frac{\eta q P_s}{h\nu} \qquad (2)$$

This is a fairly important relationship in that is can be used to calculate the quantum efficiency of a detector if the optical power and signal current are known. The minimum signal that the detector is capable of detecting is a function of the different noise sources within the system. The familiar expression for shot noise due to an average DC durrent is $N_{S1} = 2q\bar{I}BR_L$ where $\bar{I}$ is the average DC current.

The thermal noise contributed by the detector is $N_{S2} = 4KTB$, and the noise caused by the effective temperature of the following amplifier is $4KT_{eff}B$. The power signal-to-noise ratio thus becomes:

$$S/N = \frac{[\frac{\eta q}{h\nu}]^2 R_L}{2qB\ \{\frac{\eta q}{h\nu}\ (P_S+P_B) + I_D\}\ R_L + 4KB\ (T+T_{eff})} \quad . \qquad (3)$$

Now if the thermal noise dominates the shot noise (usual case for a well designed and state of the art detector), then the signal-to-noise ratio reduces to:

$$S/N = \frac{[\frac{\eta q P_S}{h\nu}]^2 R_L}{4KB\ (T+T_{eff})} \qquad (4)$$

Equations (2) and (3) are for a photovoltaic detector as generation-recombination noise is not included. Also 100% intensity modulation is assumed. Assume a 50 OHM detector operating into a matched load. The following amplifier has a 3 db noise figure. The noise equivalent power is the value of optical signal power required to produce a signal-to-noise ratio of 1. Therefore:

$$\frac{NEP}{\sqrt{B}} = \frac{2h\nu}{\eta q}\ (\frac{K\ (T+T_{eff})}{R_L})^{1/2} \quad . \qquad (5)$$

If the quantum efficiency is assumed to be 1, and the following amplifier has a noise figure of 3 db, then the

amplifier has an effective noise temperature of 290°K. Using these values (5) yields:

$$\frac{NEP}{\sqrt{B}} = 2.36 \times 10^{-12} \text{ Watts/(Hz)}^{1/2}$$

2. Heterodyne Detection Sensitivity

As with conventional radio or radar receivers, optical heterodyne detection involves the mixing of the return signal with an optical local oscillator to produce a current at some intermediate frequency; however, it is done for different reasons and produces different system results. The mean value of this intermediate current can be shown to be [Ref. 1]:

$$i_{IF}^2 = \left(\frac{\eta q}{h\nu}\right) 2 P_{LO} P_S \qquad (6)$$

The transducer gain is defined as the IF output power divided by the available signal power. Using (6) and the definition of transducer gain, it can be shown [Ref. 2] that:

$$G_T = \frac{P_{IF}}{P_S} = \frac{\left(\frac{\eta q}{h\nu}\right)^2 P_{LO}}{2[G_D (1 + G_D R_S) + \omega_{IF}^2 R_S C_D^2]} \quad . \qquad (7)$$

Thus it can be seen that the transducer gain is directly proportional to the local oscillator power. If (6) is substituted into (3) then the value of S/N becomes:

$$S/N = \frac{2\left(\frac{\eta q}{h\nu}\right)^2 P_{LO} P_S P_L}{2qB\left\{\frac{\eta q}{h\nu}\left(P_S+P_B+P_{LO}\right) + I_D\right\} R_L + 4KB\left(T+T_{eff}\right)} . \quad (8)$$

If P_{LO} is made large enough to dominate the denominator then (8) becomes:

$$S/N = \frac{\eta P_S}{h\nu B} . \quad (9)$$

Using the previous definition of NEP, it is trivial to show that:

$$\frac{NEP}{B} = \frac{h\nu}{\eta} . \quad (10)$$

This is the well known "shot noise limited operation" of a heterodyne detection system.

If the quantum efficiency is assumed to be 1 as was the example of envelope detection then:

$$\frac{NEP}{B} = 1.88 \times 10^{-20} \text{ Watts/Hz} .$$

Therefore, for a bandwidth of one hertz the heterodyne system has a theoretical sensitivity eight orders of magnitude greater than a comparable envelope detection system. Several workers have reported achieving heterodyne systems that approach within an order of magnitude of shot noise limited operation [Refs. 2, 5, and 6].

B. REQUIREMENTS FOR OPTICAL HETERODYNE DETECTION

For the relationship of (6) to represent the physical situation the signal and local oscillator wavefronts must maintain the same phase relationship over the entire sensitive area of the detector. This requirement can only be satisfied by the following conditions [Ref. 16]:

1. The two beams must have the same mode structure. The dominant TEM_{oo} mode is preferred.

2. The two beams must be spatially coincident, and to provide maximum signal-to-noise ratio, their diameters must be equal.

3. The two beam pointing vectors must be coincident. This implies angular alignment of the beams must be maintained. A quantitative discussion of this alignment will be presented in a later section.

4. The wavefront must have the same curvature. Both must be plane waves or, if curved, both must have the same radius of curvature.

5. The beams must be identically polarized so their electic vectors will be coincident.

Although these requirements appear to impose extremely stringent requirements upon the system, they can be satisfied at the longer infrared wavelengths as indicated by the experimental results cited in the discussion of heterodyne detection sensitivity.

III. GENERAL THEORY OF FM-CW RADAR

A. PRINCIPLES OF OPERATION

A radar detects the presence of targets by transmitting electromagnetic energy and absorbing the returned energy.

A conventional pulsed type radar transmits a short pulse and measures the elapsed time to the returned energy. The pulse duration and time between pulses are the controlling parameters of range resolution and the maximum unambiguous range. In a CW radar the measurable information is the target's velocity determined by the doppler relationship:

$$f_d = \frac{2v_r}{\lambda} . \qquad (11)$$

At 10.6 micrometers wavelength a velocity of 1 m/sec corresponds to a doppler shift of 188.7 kHz. Since filters of a few kHz are readily available doppler measurements of velocities to a fraction of a meter per second are readily achievable.

1. Determination of Range

A simple CW radar cannot measure range since it has no method of correlating the returned signal to the instant of its transmitted time. This inability is related to the extremely narrow bandwidth of the transmitted waveform. Some sort of timing mark must be applied to a CW carrier to allow this correlation. The more distinctive the marker, the more precise will be the range measurement

and the broader will be the transmitted spectrum. This interaction follows from the properties of the Fourier transform. One of the easiest methods to produce this timing mark is to linearly frequency modulate the CW carrier with either a sawtooth or triangular waveform.

For either case the returned signal heterodyne spectrum will consist of a $\frac{\sin x}{x}$ envelope. The spectral width will be a function of target range [Refs. 17, 18, and 19]. The closer the range the narrower will be the spectrum and hence, the greater the range resolution. This is usually the desirable condition.

The relationship between the transmitted, received, and heterodyned frequencies is illustrated in Figure 1. The heterodyne or beat frequency is determined by:

$$f_b = \frac{df}{dt} \Delta t \ . \tag{12}$$

Since the frequency deviation is linear, $\frac{df}{dt}$ can be replaced by $2f_m\Delta f$, and Δt can be replaced by the signal transit time 2R/C. Substituting and rearranging results in the range equation

$$R = \frac{Cf_b}{4f_m\Delta f} \ . \tag{13}$$

The range resolution will be determined by the combination of the IF filter bandwidth and the returned signal heterodyne spectrum.

The range resolution will be determined by the IF filter bandwidth if it is smaller than the target spectral bandwidth. If not, the target spectral bandwidth will control the range resolution.

2. Determination of Velocity

The frequency relationships of Figure 1 and the preceding discussion assumed a stationary target. If the target has relative motion with respect to the radar, a doppler frequency shift will be superimposed on the beat frequency and an erroneous range will result. Figure 2 shows the frequency relationships of Figure 1 modified by doppler information.

On one portion of the frequency-modulation cycle, the beat frequency will be either increased or decreased by the doppler frequency depending upon the sign of the relative velocity of the target. On the other portion of the cycle, the opposite direction frequency shift will be observed.

As an example, consider a closing target. During the rising portion of the transmitter spectrum, the doppler frequency will subtract from the beat frequency and during the falling portion of the spectrum, the doppler frequency will add to the doppler frequency.

$$f_b \text{ (up)} = f_r - f_d \quad \text{(a)}$$
$$f_b \text{ (down)} = f_r + f_d \quad \text{(b)} \qquad (14)$$

By summing the two frequencies the range information can be determined, and by taking the difference the velocity information can be determined. Since the two frequencies involved occur during different time increments a memory device must be utilized. High-speed counters and digital arithmetic units should be capable of performing the required functions.

If precise velocity measurements were desired, a dual mode feature could be utilized as shown in Figure 3. During the CW velocity mode, the heterodyne spectrum broadening caused by the waveforms of Figures 1 and 2 would be absent, and the velocity resolution would be limited only by the filter bandwidth of the measuring device. However, this velocity precision would not be required for most radar applications.

B. COMPARISON OF FM-CW RADAR WITH PULSED SYSTEMS

The FM-CW radar does not have the minimum range restrictions of a pulsed radar. It has the added advantage of an average to peak power of unity which is highly desirable when using a transmitter which is peak-power limited. For equal transmitted bandwidths, pulsed and FM-CW radars have comparable range resolutions [Ref. 20]; however, the pulsed type radar must have a receiver bandwidth comparable to the transmitted bandwidth. The FM-CW radar can have a receiver bandwidth which is a small fraction of the transmitted bandwidth. This implies an increased permissible receiver signal-to-noise performance and fewer permissible

stages of amplification due to the gain-bandwidth product.

To change range resolution in the FM-CW radar, one merely has to change the transmitted frequency deviation. To produce a comparable change in a pulsed system, one generally would have to change the pulse width, pulse repetition frequency, and the receiver bandwidth.

For equal average transmitted powers, target illumination times, receiver noise figures, antenna gains, integration efficiencies, and optimized bandwidths, pulse and FM-CW radars have comparable maximum range capabilities [Refs. 18 and 20].

IV. OPTICAL MODULATION

A. GENERAL CONSIDERATIONS

Since the phase velocity of an electromagnetic wave is a function of the index of refraction of the medium through which it passes, any material whose index of refraction can be varied can be used to modulate an optical beam.

If the index of refraction is varied by means of an electric field by the Pockels or Kerr effect, then it is known as an electrooptic modulator. By various physical configurations this type of modulator can be used for intensity, phase, polarization and deflection modulation [Refs. 21 and 22]. If the index of refraction is varied by a magnetic field, it is known as a magnetooptic modulator. Here the prime mechanism is a rotation of the wavefront polarization and hence, it is not suitable for intensity or frequency modulation. If the index of refraction is varied by a mechanical force (pressure), it is known as an acousto-optic modulator. The mechanism is the diffraction of an optical wave by a traveling acoustic wave. The diffracted wave is not only deflection modulated, but it is also simultaneously frequency modulated.

B. ACOUSTO-OPTIC MODULATION

An explanation of the interaction of light and sound can be obtained through the dual particle-wave nature of light and sound energy [Ref. 23].

Using this approach a light beam with a propagation vector $\vec{K}$ and a frequency ω can be considered a stream of photons with momentum $\hbar\vec{K}_L$ and energy $\hbar\omega$. In a like manner the sound beam is modeled as photons with momentum $\hbar\vec{K}_s$ and energy $\hbar\omega_s$. Since the momentum and energy of the system must be conserved, the propagating vector of the diffracted wave must be:

$$\vec{K}_o = \vec{K}_L + \vec{K}_s \quad \text{and the frequency must be:}$$

$$\omega_o = \omega_L + \omega_s \ .$$

Figure 4 shows the required momentum conservation and the resultant direction of propagation of the diffracted beam.

Figure 5 is a schematic diagram of a basic acousto-optic modulator. Note that if the optical beam is orthogonal to the acoustic beam, a zero-order beam (unmodulated), first order diffracted beams (modulated by the acoustic frequency), and higher order beams (not shown) will result.

If the optic and acoustic waves are offset from the orthogonal condition by the bragg angle as shown in Figure 6, a zero order and higher order diffracted beams in a single direction only will be observed. For this case, the energy of the single first order diffracted beam will be twice that of a single order diffracted beam of the basic modulator. The frequency modulation will be

the same. Diffracted beams of higher order than the first are usually neglected due to the extremely low energy content. For a more detailed explanation concerning bandwidths, optical demands, power requirements and general parameters, see Refs. 4, 24, 25, 26 and 27.

V. GENERAL SYSTEM ASPECTS OF A 10.6 μ LASER RADAR

On a macroscopic scale a radar consists basically of a transmitter, a receiver and a propagation medium through which the electromagnetic energy must pass. For the purpose of this discussion the laser will be viewed solely as a radar transmitter. Only those parameters that pertain to system performance will be considered. The receiver can be considered to consist of an optical antenna, detector and associated signal processing. Since the majority of the important detector characteristics have already been covered, this section will discuss the antenna or optical considerations.

A. LASER RADAR TRANSMITTER

Since the acousto-optic modulator is polarization sensitive, the laser transmitter should be polarized and have a polarization corresponding to maximum efficiency of the modulator.

Previous discussions indicated that the transmitter and LO beams should have the same spatial coherence. For maximum signal-to-noise ratio and ease of alignment, this coherence should be restricted to the dominant TEM_{oo} mode of propagation. Additional restrictions are minimal for systems deriving the transmitted and local oscillator beams from a single laser source.

B. ATMOSPHERIC PROPAGATION

The medium through which an optical beam travels has a significant effect on the system performance. Absorption and scattering by the atmospheric constituants and suspended aerosols must be considered for a homogeneous medium. In the more usual case of a turbulent medium, the additional system perturbations of the beam shape, dimensions and electromagnetic properties must be considered.

1. Absorption

The fraction of an optical beam intensity passing through a transmission medium is proportional to the distance traveled [Refs. 3 and 8]. Stated mathematically this becomes:

$$\frac{dI}{I} = -K_A dL \ .$$

Solving for I results in:

$$I(x) = I_o e^{-K_A L} \quad . \tag{15}$$

A number of different atmospheric constituants attenuate an infrared beam as it passes through the atmosphere. The primary effect can be attribuyed to water vapor (H_2O), carbon dioxide (CO_2) and ozone (O_3) (high altitudes only). Considerably lesser effect may be observed from methane (CH_4), nitrous oxide (N_2O), and carbon monoxide (CO) if the path is long. The amount of water vapor in the path varies over a wide range, and while

the carbon dioxide is mixed more nearly uniformly, it may still vary appreciably in various air masses. Thus a detailed knowledge of the meteorological conditions is necessary to perform an exact calculation of the infrared transmission. Even though such detailed information is seldom, if ever, available it is usually possible to make gross predictions using such meteorological parameters as temperature, pressure and relative humidity. Early workers performed many field measurements over typical paths and under a variety of weather conditions. Results of these measurements in graphical and tabular form are available [Refs. 8 and 9], and are of value to the system engineer who must estimate the system performance under field conditions.

2. Scattering

Scattering has the same intensity as a function of path length relationship as absorption. The effect of scattering on infrared transmission can, therefore, be represented by (15) with the absorption coefficient K_A replaced by the scattering coefficient K_S. The total transmittance of the path can be represented by:

$$\tau = e^{-\sigma L} \tag{16}$$

where $\sigma = K_A + K_S$ and is known as the extinction coefficient.

Two major models for scattering exist. If the scattering particle is considerably smaller than the optical wavelength, it is known as Rayleigh scattering. Here the

scattering coefficient is inversely proportional to λ^4. As such, shorter wavelengths are scattered much more than longer wavelengths, and for all practical purposes Rayleigh scattering can be neglected at 10.6 micrometers. The second model occurs if the size of the scattering particle is comparable to, or larger than, the optical wavelength.

Mie scattering can be described by the following empirical relationship [Ref. 4]

$$K_S = \frac{3.91}{V} \left[\frac{\lambda}{.55}\right]^{-.585V^{1/3}} \tag{17}$$

where V is the visual range in kilometers, the wavelength is in microns, and the path length is in kilometers. If the scattering centers are spherical, the relationship:

$$K_S = \pi n \gamma r^2 \tag{18}$$

can be used where γ is the scattering area ratio and is a measure of the efficiency with which a center scatters the incident energy. n is the number of scattering centers per cubic centimeter and γ is the radius of the scattering center. Figure 7 shows the relationship between γ and the ratio of the scattering center radius to wavelength (r/λ). Notice that the center is the most efficient scatterer when the center radius size is approximately equal to the wavelength. Measurements of the droplets in fogs show that their radii

range from 0.5 to 80 microns. The peak of their size distribution usually occurs between 5 and 15 microns. Therefore, fog particles are efficient scatterers at the 10.6 micron wavelength [Ref. 9].

3. Beam Distortion

In the presence of a turbulent propagation medium, the beam may be distorted in several different ways. These beam distortions may appreciably affect the system performance. This turbulence which is a manifestation of thermal and pressure inhomogeneities causes a change in the index of refraction of the medium. The changes in the index of refraction modify the propagation constant and Poynting vector of the optical beam and this modification can be summarized as follows [Ref. 28]:

a. Beam steering - angular deviation from the line of sight path.

b. Image dancing - variations in the angle of arrival of the beam wavefront.

c. Beam spreading - small angle spreading which increases the beam divergence.

d. Beam scintillation - small-scale destructive interference within the beam cross section.

e. Spatial coherence degradation - losses in phase coherence across the beam phase front.

If the turbulent medium is modeled as consisting of discrete blobs, each homogeneous but with a different index of refraction from adjacent blobs, then the relative

size of the optical beam and the turbulent blobs will determine which of the above distortions will predominate. If the blob size is ℓ and the beam size is d_B, then for $d_{B/\ell} << 1$ the major effect will be beam steering and image dancing. For $d_{B/\ell} >> 1$, the major effect will be beam spreading, beam scintillation, and spatial coherence degradation.

Numeric models of a turbulent medium have been developed by Tatarski [Ref. 29]. In Tatarski's model, the degree of atmospheric turbulence and its relationship to the optical properties of the atmosphere can be characterized by a structure constant for refractive index fluctuations, $C_n(r)$. The value of the structure constant varies with altitude and time of day. Typical values for daytime conditions near the earth are:

Weak turbulence - $C_n(r) = 8 \times 10^{-9}\ m^{-1/3}$

Intermediate turbulence - $C_n(r) = 4 \times 10^{-8}\ m^{-1/3}$

Strong turbulence - $C_n(r) = 5 \times 10^{-7}\ m^{-1/3}$

If the smallest inhomogeniety blob is ℓ_o, the largest is L_o, and the path length is L, then the fluctuations in phase between points of the wavefront separated by the distance ρ, as postulated by Tatarski, can be represented by:

$$\sigma_\phi^2(\rho) = \begin{cases} 1.46\left(\frac{2\pi}{\lambda}\right)^2 \rho^{5/3} \int_o^L C_n^2(r)dz & \text{for } \ell_o < \rho < (\lambda L)^{1/2} \\ 2.91\left(\frac{2\pi}{\lambda}\right)^2 \rho^{5/3} \int_o^L C_n^2(r)dz & \text{for } L_o > \rho > (\lambda L)^{1/2} \end{cases} \quad (19)$$

The first condition leads to beam spreading, beam scintillation, and spatial coherence degradation. The second condition leads to beam steering and image dancing. Figure 8 shows the lateral phase coherence length as a function of path length for intermediate turbulence. Figure 9 shows the phase front angle of arrival deviation as a function of beam diameter for intermediate turbulence.

Fried has derived an expression for the degradation in the signal-to-noise ratio for an optical heterodyne receiver in terms of the relative sizes of the receiver aperture, d_R, and the phase coherence dimension, r_o [Ref. 30]. An examination of his derivation reveals that little improvement in the signal-to-noise ratio will result by increasing the receiver aperture beyond r_o. The quantity r_o is related to the transmission wavelength, zenith angle, θ, and receiver altitude, H_o, by the relationship:

$$r_o = .05\ [\lambda]^{6/5}\ \cos^{3/5}(\theta)\ \left[\frac{\Gamma(2/3)}{\Gamma(2/3\ \frac{Ho}{3200})}\right]^{3/5} \qquad (20)$$

where $\Gamma(x,y)$ is the incomplete Gamma function [Ref. 31]. The coherence dimension can also be related to Tatarski's atmospheric structure constant by [Ref. 31].

$$r_o = 1.2 \times 10^{-8}\ (\lambda)^{6/5}\ (L)^{-3/5}\ (C_n(r))^{-6/5} \qquad (21)$$

From the $\lambda^{6/5}$ dependence of r_o, it can be seen that the coherence dimension is about 30 times greater for 10.6 μ than for .63 μ.

The $\lambda^{6/5}$ dependence of r_o has been experimentally verified and reported by Gilmartin and Holtz. Their measurements encompassed wavelengths from the visible through 10 microns under conditions of medium and severe atmospheric degradation of resolution [Ref. 32].

In addition, they have shown that focused beam size and focused beam wander can be predicted from relatively simple visual resolution measurements. Additional theoretically predicted and experimentally verified methods of determining the degree of coherence of a laser beam passing through a turbulent medium has been reported by Grant and Ageno [Ref. 33]. This work presents the relationship between the mean square angular deflection of a laser beam and the corresponding degree of coherence of the wavefront.

C. RECEIVER OPTICS

An optical heterodyne receiver can be separated into two separate components: an optical antenna and an optical receiver. Since the important aspect of receiver sensitivity has been discussed in a previous section, this section will consider the directional characteristics and spatial requirements of an optical antenna.

1. Unfocused Heterodyne Detection

If the local oscillator and signal beams are both colimated (plane wavefront) and spatially misaligned as shown in Figure 10, the following mathematical model of heterodyne signal spatial degradation can be developed [Refs. 3 and 4].

Assume the detector to be an ideal square law device. If the signal and local oscillator fields respectively are:

$$E_S(t) = A_S \cos\left(\omega_S t + \Phi_S - \frac{\omega_S x}{v_x}\right)$$

$$E_L(t) = A_L \cos\left(\omega_L t + \Phi_L\right)$$

then the instantaneous detector input signal will be equal to

$$S(t) = \left[A_S \cos\left(\omega_S t + \Phi_S - \frac{\omega_S x}{v_x}\right) + A_L \cos\left(\omega_L t + \Phi_L\right)\right]^2 \quad (22)$$

The intermediate or heterodyne signal component is determined by performing the squaring operation and applying trigonometric operations. If this is done, the detector heterodyne current will be the time average and spatial integral over the detector surface.

$$i_{IF} \propto \iint_{AREA} \cos\left(\omega_{IF} + \Phi_S - \Phi_L + \frac{\omega_S x}{v_x}\right) dA \quad (23)$$

Performing the integration yields

$$i_{IF} \propto A_S A_L \cos\left(\omega_{IF} + \Phi_S + \Phi_L\right) \frac{\sin\left(\omega_S d/2v_x\right)}{\left(\omega_S d/2v_x\right)} \quad (24)$$

If the signal degradation due to misalignment angle ψ is to be kept less than 10%, then the term $(\omega_S d/2v_x)$ must be less than .8 radian. By making the substitution

$v_x = \frac{C}{\sin \psi}$ it can be shown that $\psi \lesssim \frac{\lambda}{4d}$ must be maintained. The first null in the heterodyne signal will occur for

$$\frac{\omega_S d}{2v_x} = \frac{\frac{2\pi Cd}{\lambda}}{\frac{2C}{\sin \psi}} = 3.14 \quad . \qquad (25)$$

or $\sin \psi = \frac{\lambda}{d}$. For small ψ, $\psi \approx \frac{\lambda}{d}$.

If a 5 mil x 5 mil detector is assumed, then

$$\psi = \frac{10.6 \times 10^{-6} m}{1.27 \times 10^{-4} m} = 83 \text{ milliradian} \ .$$

Of course, the obvious disadvantage of this simple receiver is the extremely small intercepted signal energy and hence poor receiver signal-to-noise ratio.

2. Simultaneously Focused Beams with a Single Aperture

Corcoran has performed an analysis of heterodyne detection with focused signal and local oscillator beams by a single aperture [Ref. 34]. His analysis assumes that the focusing element is in the Fraunhofer region or far field of the light sources. As in the previous analysis, this assumes that the light incident upon the aperture is effectively a plane wave. Figure 11 is a representation of the detection process. His results show that

$$i_{IF}(t) \propto \cos \omega_{IF} t \sin \frac{[(\sin \theta_2 - \sin \theta_1)(\pi d_A/\lambda)]}{\pi S' (\sin \theta_2 - \sin \theta_1)} \qquad (26)$$

when $\theta_1 = 0$, the first zero of the heterodyne current occurs when $\sin(\theta_2) \frac{\pi d_A}{\lambda} = \pi$. For small values of θ_2 this reduces to $\theta_2 = \frac{\lambda}{d_A}$.

Focusing with a single aperture, therefore, decreases the receiver field of view when the receiving aperture is larger than the detector. Corcoran's analysis of Fraunhofer region unfocused detection agrees with Refs. 3 and 4.

Additional theoretical predictions relating the receiver aperture, wavelength and angular field of view have been presented by Siegman [Ref. 35]. By several methods he has shown that the product of the effective receiver aperture, A_R, and the solid angle field of view, Ω_R, are approximately constant and related by

$$A_R \Omega_R \approx \lambda^2 . \tag{27}$$

By making the substitution $\frac{\Omega_R}{4\pi} = \frac{\pi(\frac{R\theta}{2})^2}{\pi R^2}$ it can be seen that for a circular aperture of diameter d_A

$$\theta = \frac{2\lambda}{\pi d_A} . \tag{28}$$

This is in good agreement with Corcoran's results.

3. Signal Beam Only Focused

Read and Turner have presented theoretical calculations and experimental verification of an optical heterodyne

technique which greatly reduces the stringent angular requirements [Ref. 36]. In this method the signal beam is focused with a diffraction-limited lens or mirror. A colimated local oscillator beam is superimposed on the resulting Airy pattern and optical heterodyning results. The Airy disk and local oscillator beam can interact efficiently because both wavefronts will be plane [Ref. 23]. The greatest heterodyne efficiency and signal-to-noise ratio will be achieved if only the central disk of the Airy pattern is used. This is due to phase reversals of the successive diffraction rings.

The electric field strength due to the signal beam in the focal plane is

$$E_S(t) = A_S \cos(\omega_S t + \Phi_S) \frac{J_1(\alpha r)}{(\alpha r)} \qquad (29)$$

in which

$\alpha = 2\pi a/\lambda f$

a = lens radius

f = lens focal length

r = radius from disk center

$J_1(x)$ = Bessel function of order one

R = disk radius.

At a distance ℓ from the axis, the two wavefronts are out of phase by $\frac{2\pi\phi\ell}{\lambda}$.

The elemental signal is, therefore, proportional to

$$di_{IF} \propto A_S A_L \cos(\omega_{IF} t + \Phi_S - \Phi_L) \cos\left(\frac{\pi\phi\ell}{\lambda}\right) . \qquad (30)$$

The total signal is obtained by integrating over the area of the Airy disk.

This integral is not expressive in elementary functions for finite disk sizes, but if the assumption is made that the signal beam intensity is uniform over the disk area, then the integral results in

$$i_{IF}(t) \propto \frac{A_S A_L}{\phi} R J_1 \left(\frac{2\pi\phi R}{\lambda}\right) . \qquad (31)$$

Now if the substitution $R = 1.22 \lambda f/d_A$ is made, the voltage signal-to-noise voltage ratio can be expressed as

$$(S/N)_V = \frac{K J_1 (2.44\pi\phi f/d_A)}{\phi} \qquad (32)$$

The first zero will occur for $\phi = .5\frac{d_A}{f}$. If the optics has a speed of f/(no) of 10, then the angular field of view will be 50 mrad. This reduced angular requirement is not without restrictions, however, since the center of the focused spot must not deviate from the center of the aperture in the focal plane by more than a fraction of its diameter.

VI. DEVELOPMENTAL HETERODYNE DETECTION FM-CW RADAR

A. SYSTEM DESCRIPTION

Two optical configurations were constructed and tested for the developmental system. Figures 37 and 38 are photographs of the physical optics utilized. Several high-quality photovoltaic detectors were available and each was tried in the two-system configurations.

1. Basic System Block Diagram

The over-all system block diagram is shown in Figure 13. Equipment model numbers and component parameters are given in Appendix A. The system optics (two separate configurations) are shown in more specific detail in a subsequent section.

2. Major Component Description

a. Laser

The laser used for the developmental system was a Honeywell model 3000 three-watt continuous wave CO_2 laser. The laser output was vertically polarized, and output power was continuously controllable over a range of .2 - 3 watts. A piezoelectric transducer (PZT) was attached to the rear cavity mirror for control of the selected radiation line although this feature was not used for the described system. The laser was a sealed cavity type and was water-cooled. The water flow requirement was about .25 gallons per minute.

b. Modulator

The 10.6 micron AO modulation system consisted of three main components: a water-cooled Germanium AO modulator; a pair of Germanium focusing lenses, each with a 5" focal length; and a combination voltage controlled oscillator (VCO) and RF power amplifier. This latter combination will be collectively referred to as the modulator driver. The modulator driver was capable of supplying six watts of CW power to the modulator. The bandwidth of the modulator system was measured and found to be in excess of 20 MHz. The output frequency linearity as a function of modulator driven DC control voltage input was measured and it was found that non-linearities existed above 45 MHz and below 35 MHz. The effective bandwidth of the modulator for this system was concluded to be 10 MHz.

c. Detectors

Three detectors were used during the system tests. All three detectors were of the PbSnTe photovoltaic type. One detector was a Raytheon IR-101 PN photovoltaic detector packaged within a glass dewar. The other two detectors were Rockwell International PIN photovoltaic detectors packaged within stainless steel dewars. Pertinent detector parameters are given in Appendix A.

3. Theory of Operation

Refer to Figure 13 for the following description of system operation. The bias supply V_b determine the center frequency of the modulated optical beam. Since the

linear bandwidth of the modulation systems extends from 35-45 MHz, the value of V_b was set to -7.5 volts corresponding to a center frequency of 40 MHz. The sweep voltage was obtained from a function generator and passed through a high-pass filter. It was adjusted for an amplitude to produce a frequency sweep from 35-45 MHz out of the modulator driver. Since the laser output beam is frequency swept in a triangular fashion, the detected laser return will also be frequency swept in a triangular fashion from 35-45 MHz. This detected signal is amplified by a combination of wideband amplifiers resulting in 53 db of amplification prior to insertion of a balanced mixer. The output of the VCO is available at the DC input to the modulator driver and was extracted by a high-pass filter. This filter passes the 35-45 MHz swept signal while blocking the much lower frequency sweep voltage. The 35-45 MHz swept signal is mixed in a double balanced mixer with a 30 MHz signal and translated to 65-75 MHz. This signal is then passed through a 60 db wideband amplifier to raise the signal to the proper level to drive the "L" port of a double balanced mixer. The 65-75 MHz filter eliminates all undesirable mixer products from mixer number 1. If the detected signal and the "L" port signals of mixer 2 were sweeping from 35-45 MHz and 65-75 MHz, respectively, in synchronism (zero range and zero doppler), then a single output frequency of 30 MHz would be observed. As the range is increased, the 30 MHz signal splits into two distinct

frequencies, one above and one corresponding below 30 MHz. The frequency shift from 30 MHz is proportional to the range. Doppler information manifests itself in a shift of the signal pair centroid from 30 MHz. The mathematical relationship describing these phenomena was presented in Chapter III, A, sections 1 and 2.

4. Optical Configurations

Two system optical configurations were tried. The first configuration was initially tried at the Naval Electronics Laboratory Center (NELC) in May 1974 during the author's industrial experience tour. Refer to Figure 14 for a description of this configuration. The designation x/y refers to a beam splitter and means x per cent of the beam energy is reflected by the beamsplitter and y per cent is transmitted by the splitter. Ninety per cent of the laser beam is reflected to become the radar output beam. The 5" focal length lens prior to the AO modulator focuses the beam to a small waist size to increase the modulator bandwidth. The 5" focal length lens after the AO modulator colimates the two emerging beams and restores the output beam divergence. The blocking aperture passes the modulated beam and blocks the zero-order beam. The 50/50 splitter following the blocking aperture passes 50% of the output beam and also reflects 50% of the return beam down to the detector. The 5/95 splitter in the output path passes 95% of the output signal and returned signal but reflects essentially 100% of the visible He-Ne beam. Fine

adjustment of this splitter superimposes the CO_2 and He-Ne beams, and hence the radar output beam can be aimed according to the visual beam. The output mirror is adjustable in both vertical and azimuth and facilitates the steering process. The mirror in the He-Ne path has a small hole near the center through which the visible beam passes. By aiming the telescope at the front surface of this mirror, the telescope reticles can be precisely aligned with the illuminated area. The local oscillator beam is the beam transmitted through the 90/10 splitter. It is folded three times with the front surfaced mirrors and passed through a limiting aperture. This aperture controls the amount of local oscillation power incident upon the detector. The 5/95 splitter just prior to the 8" focal length lens passes 95% of the returned energy and 5% of the local oscillator energy. It is adjusted to superimpose the signal and local oscillator beams. The 8" focal length lens focuses both the local oscillator and signal beams to an Airy disk comparable to the detector size. The absorber absorbs that portion of the transmit beam reflected by the 50/50 splitter. This power is appreciable and oculd become a health hazard if it were not blocked.

The second optical configuration is shown in Figure 15. This configuration was constructed to overcome two distinct disadvantages of the first system. The 50/50 splitter attenuates 3 db of the output beam and also 3 db on the receive path, hence elimination of this splitter

should immediately cause a 6 db increase in system performance.

An increase in the receiver aperture would also cause an increase in the system performance; hence a simple Newtonian antenna system was chosen. The path through the modulation system is essentially unchanged. The zero order blocking aperture was replaced by a folding mirror and the zero order beam was used as the local oscillator beam. Beam elevators had to be used to raise the local oscillator and signal beams to a height required by the larger diameter of the receiver optics. The small front obstruction mirror was double surfaced. The output beam was reflected from the front surface, and the returned signal was reflected from the rear surface. This was an elliptical mirror measuring 1-1/2" by 2-1/4". The primary reflecting mirror was a 6" diameter mirror with a 60" focal length. Notice that the local oscillator beam was unfocused. The visual alignment mechamism was the same as in the previous configuration.

B. EXPERIMENTAL PROCEDURES

1. Modulator Measurements

Parameter measurements of the basic system components consisted of modulator frequency deviation and power output of the modulated beam as a function of VCO driver voltage. The deflection efficiency and over-all transmission efficiency was measured at the center of the effective

bandwidth (40 MHz). Figure 16 shows the modulation linearity as a function of VCO driving voltage. Figure 17 shows the modulated and zero order beams after the colimating lens. This figure is the result of recording the spatial intensity patterns of the beams on temperature-sensitive paper. The Bragg angle for this moudlator at 10.6 microns was approximately 2.21 degrees. The modulator was mounted on a stand with x, y, z and Bragg angle micrometer adjustments, and each dimension was adjusted for maximum power output of the modulated beam. The zero order beam was blocked with an aperture. The power input to the modulator, and the modulated beam and zero order diffraction beam powers were measured at 40 MHz. If the deflection efficiency (DE) is defined as:

$$DE = \frac{\text{Power in Modulated Beam}}{\text{Total Power Output}}$$

and the transmission efficiency (TE) is defined as:

$$TE = \frac{\text{Power Output}}{\text{Power Input}}$$

then the resultant measured efficiencies were a deflection efficiency of 53% and a transmission efficiency of 55%.

2. Alignment Procedures

The alignment procedures for the two optical configurations were appreciably different; therefore, each procedure will be discussed separately.

a. First Optical Configuration

Refer to Figure 14 for this discussion. Prior to insertion of the AO modulator, the 90/10 splitter was adjusted to produce a 90° beam reflection which was parallel with the optical table top. After the AO modulator was inserted, it was adjusted for maximum power in the modulated beam. The colimation lens was adjusted to produce a constant separation of the modulation and zero order beams over the length of the optical table (distance of about three feet). The blocking aperture was then adjusted to allow unobstructed passage of the modulated beam and total blockage of the zero order beam. The 50/50 and 5/95 splitters and steering mirror were positioned such that the output beam struck each as closely as possible to the center. The He-Ne laser was adjusted for coincidence of the He-Ne and CO_2 beams at a distance of approximately 40 feet from the steering mirror. For CO_2 beam powers of approximately .25 watts or greater the beam was sensed with temperature-sensitive chart paper (see Figure 17). For CO_2 beam powers of a few milliwatts to approximately .25 watts, the beam was sensed with temperature-sensitive liquid crystal paper. The liquid crystal paper was able to detect approximately one milliwatt at the focal plane of the 8" focal length lens. The 5/95 splitter in the receive path was placed to allow maximum transmission of the received signal while simultaneously reflecting the local oscillator beam. These two beams were adjusted to be as coaxial as possible at the exit surface

of the 5/95 splitter. The focusing lens was positioned such that both beams were concentric with the lens center. For precise alignment between the signal and local oscillator beams a folding mirror was placed approximately 20 feet from the folding mirror, and it was adjusted to precisely fold the visible beam back upon itself. The 50/50 splitter and the 5/95 splitter in the receive path were then adjusted to provide coincidence of the signal and local oscillator beams at the focal point of the detector focus lens. As a final precision adjustment a pinhole aperture (approximately .01 inch diameter) was placed at the focal point of the lens and the two beams were adjusted to pass through the aperture. Every time this procedure was followed, there was sufficient beam overlap to produce heterodyne operation. Once heterodyne operation was achieved, fine adjustment of the beam splitters to produce a maximum signal-to-noise ratio was easily achieved. The detector was placed at the lens focal point by inserting a "whisper" fan just prior to the detector. The detector was then raster scanned until the low frequency (approximately 100 Hz) "chopped" signal was observed on an oscilloscope. The detector was then positioned to produce a maximum chopped signal.

b. Second Optical Configuration

Refer to Figure 15 for this discussion. The alignment procedure through the modulator was the same as for the first configuration. The transmit beam elevator

was adjusted to place the transmit beam in the center of the front face of the elliptical obstruction mirror of the Newtonian antenna. The He-Ne and CO_2 beams were adjusted to be coaxial as in the first configuration. A two-inch diameter gold surface retro-reflector was placed on the top of Ingersoll Hall. With the 5/95 splitter removed, the visible return from the retro-reflector could be seen on the dewar window. By chopping the returned signal, the detector could relatively easily be placed at the antenna focal spot. Once the chopped signal was located, the 5/95 splitter was set in place. The detector would then have to be moved horizontally to compensate for the beam offset caused by the beam splitter. This was always accomplished with relative ease. A small folding mirror was placed after the modulator and its height was adjusted to fold the zero order beam while passing the modulated beam. The zero-order beam was folded parallel to the transmit beam and adjusted in height and direction to strike the center of the 5/95 splitter. The 5/95 splitter was then adjusted to produce a maximum chopped local oscillator signal at the detector. Since the local oscillator beam was unfocused, this task was relatively simple.

C. EXPERIMENTAL RESULTS

The aforementioned systems were constructed and aligned in Spanagel 704. This was a seventh-story location with open-window access to both land and sea targets. Initial

tests were conducted over path lengths of several meters to 70 meters on the roof of Spanagel Hall with the aid of several folding mirrors. The majority of the tests were conducted several times, and in all cases the results were highly reproducible. Initial feasibility tests of the first optical configuration, less the processing electronics, were conducted during the author's experience tour at NELC (Code 2500) during May 1974. Subsequent testing was over the period of July to December 1974.

1. Zero Range Error

Two distinct and related effects will be discussed in this section. During the initial radar feasibility tests conducted with the optic configuration of Figure 14, a 40 MHz heterodyne signal was observed when the detector was illuminated by the local oscillator alone. This is an extremely troublesome effect for a CW radar with a stationary target since a signal is present at the detector whether a target return is present or not. It was postulated that this effect was caused by a portion of the modulated beam being reflected by the exit surface of the AO modulator and entering the local oscillator beam by one of two mechanisms. These mechanisms could be: reflections of the AO reflected beam from the front face of the laser, or internal laser cavity amplifications of the AO reflected beam which would then appear superimposed on the local oscillator beam. The following remedy verified the reflection source and eliminated its effect. A quarter wave plate was inserted between the

90/10 splitter and the AO modulator. A wire grid polarizer was inserted in the local oscillator path and adjusted to the polarization plane of the local oscillator. The effect of the quarter wave plate was to shift the polarization of the reflected beam orthogonal to the incident beam. The wire grid polarizer was then able to pass the true local oscillator beam while blocking the reflected beam. Although this remedy reduced an average heterodyne signal-to-noise ratio of 40 db to 2-3 db and verified the source of the initial reflections, it contributed no further evidence as to the mechanism by which the reflections entered the local oscillator beam.

When the system was moved to NPS and reconstructed, no detectable local oscillator contaminating signal could be detected for the first two weeks of laser operation. During the interim period between initial tests at NELC and the resumption of testing at NPS, the laser cavity had been recharged to restore the laser power output to the proper level. After a laser use period of about two weeks, the local oscillator contaminating signal reappeared. Its characteristics were somewhat altered from those originally observed at NELC. The contaminating signal strength and frequency response were a function of laser operating time. In general, when the laser was first energized, the contaminating signal would be absent and would appear after about five minutes of laser operation.

De-energizing the laser for a period of 10-15 minutes before re-energizing resulted in fairly reproducible results. Figures 22, 23, 24, and 25 show the amplitude and frequency response of the contamination signal as a function of laser energized time. Although these tests were by no means conclusive, it was strongly suspected that the local oscillator entry mechanism was via laser cavity amplifications since the laser cavity gain curve and frequency response are a function of laser cavity temperature and pressure.

The zero range offset was caused by the finite time delay for the acoustic wave to propagate from the PZT launch location to the optical beam waist location. This delay varies as to the physical location of the optical beam within the AO modulator optical input aperture. However, once the optical system is adjusted, the delay remains fixed, and it can easily be accounted for when computing range and velocity information. Figure 26 shows the system presentation with no signal return. The zero range offset is visible via the previously discussed local oscillator contaminating signal.

2. Range Measurement

Initial range measurements of a stationary target were performed on the roof of Spanagel Hall with folding mirrors. The range to each target location was accurately measured, and the resulting beat frequency was recorded.

During this measurement phase the zero offset range was not clearly visible, and initial confusion concerning the range measurements resulted. Since the short range specular reflector targets yielded a large signal return, the Raytheon IR-101 detector was used in conjunction with the optical configuration of Figure 14. No photographs of the system presentation were taken during this measurement phase; however, Table 1 and Figure 19 are the results of these measurements. Figure 19 gives the value of the zero offset range. Using the relationships of Chapter III, Section A.1, the range information was easily computed by

$$R = \frac{Cf_r}{4f_m\Delta f}$$

where f_r = frequency shift observed minus the zero range offset frequency.

The second phase of the stationary range measurements was conducted at a range of approximately 305 yards. The target was a 2" diameter, gold-surfaced retro-reflector. The target was placed on the roof of Ingersoll Hall. Figures 18 and 21 show the propagation path for this measurement phase. The optical configuration of Figure 15 in conjunction with the Rockwell Internation number 5-128-4 detector (on loan from NELC) was used. Figure 26 clearly shows the amount of zero range offset to be about 37 KHz. Figure 27 shows the unprocessed detector output, and Figure 28 shows the processed presentation. Note that

Figure 28 also shows the zero range offset at a much reduced amplitude. Using the system parameters given below, the range was computed to be 295 yards.

Transmit Frequency Deviation	35-45 MHz
Modulation Frequency	1.75 KHz
Target Range	305 yards
Observed Range Frequency	100 KHz.

The retro-reflector was next moved to the edge of El Estero Lake for range measurements. This range was considerably beyond 300 yards. Although the exact range was unknown, a visual estimation of the range was 1000-1200 yards. The retro-reflector was easily acquired, and a S/N ratio of 35 db resulted. The corresponding measured range frequency was 260 KHz including the zero range offset. This computed to a range of 1055 yards. Since the received signal power is a R^{-4} relationship, the S/N ratio should have decreased approximately 21 db. Allowing a several additional db decrease for atmospheric transmission effects, the results were well within expectations.

The longest range attempted was from Spanagel Hall to the U.S. Coast Guard Pier. This range was approximately 2400 yards to the end of the pier. Target acquisition was somewhat more difficult than for the El Estero Lake measurements, and this was attributed to misalignment of the visible and CO_2 transmit beams and the narrow receiver field of view. The measured data were a S/N ratio of 20 db and a range frequency of 540 KHz including the zero range

offset. This computed to a range of 2370 yards which was in excellent agreement with the known value. The range difference from 305 yards should have caused a S/N reduction of approximately 36 db. If several db were allowed for atmospheric losses, the results again were well within expectations. Figures 29 and 30 show the spectrum analyzer display of the signal return from the Coast Guard pier. Figure 20 shows the local area map and the signal paths used for the El Estero Lake and Coast Guard pier range measurements.

3. Velocity Measurements

A velocity measurement experiment was conducted to demonstrate that the target's relative velocity could be measured, and that this measurement could be accomplished simultaneously with the range measurement. To accomplish this measurement, a model train was set up on the roof of Ingersoll Hall. The track was oval with one of the straight segments parallel to, and illuminated by, the CO_2 radar beam. An electric timer in conjunction with a meter stick was used for elapsed time velocity measurements. Both up and down doppler informations were obtained by reversing direction of the train. Figures 31 and 32 show the experimental set-up used for these measurements. These figures also show the target retro-reflector that was used for the majority of the target informations. Due to the mechanical nature of the apparatus, the velocity measurements were

rather imprecise. Due to elevation differences between the transmitter and target locations, a correction factor of cos 5.5° must be applied to compute the horizontal velocity of the train. Figures 33, 34, 35 and 36 and Table 2 are the results of this experiment. The figures clearly indicate that simultaneous velocity and range measurements are possible. The direction of velocity was immediately apparent, and the computed magnitude was well within the experimental error of the apparatus.

Although this experiment demonstrated the range and velocity determination capabilities of the system as expected, an unexpected phenomenon was observed with the optical configuration of Figure 15. In addition to the expected doppler shift of the two range frequencies, the stationary target range frequencies were also present. They were, however, at a reduced amplitude. The experiment was conducted several times under varying conditions and essentially the same results were obtained. Figures 31, 34, 35, and 36 show the simultaneous presence of both the stationary target and moving target signals. The target was clearly in motion while these photographs were taken; also, the signal was definitely from the moving retro-reflector and not from the train track or any other adjacent stationary target. The experiment was essentially repeated at a later date with the optical configuration of Figure 14. The range and velocity results were as expected; however, the

stationary target frequencies were no longer present. No cause for this unexpected phenomenon has been postulated. An additional puzzle is why it should appear with one optical configuration and not with the other.

4. Receiver Field of View

The receiver field of view measurements were conducted at 305 yards using the retro-reflector. The retro-reflector was positioned to maximize the returned signal. The retro-reflector was then moved a known distance and the resulting S/N ratio was recorded. Two receiver fields of view were calculated: one at the point where the S/N ratio decreased by 3 db and one where the S/N ratio was reduced to unity. The results are given below:

Optical Configuration of Figure 14

S/N reduced by 3 db	S/N reduced to unity
Not Recorded	7.4 m radian

Optical Configuration of Figure 15

S/N reduced by 3 db	S/N reduced to unity
179 μ radian	6.8 m radian

An additional rough measure of the receiver field of view was conducted at the 1055 yard range. The arc-length which resulted in a S/N ratio of unity was approximately one yard. This resulted in a field of view of .95 m radian. A comparable decrease of 35 db S/N ratio

at 305 yards results in a field of view of .65 m radian. Although all of these measurements are indicative of the system performance, the most useful are most likely the 3 db figures.

The analysis of Chapter V, Section C.2 most closely represents the physical system utilized. The 3 db field of view of the optical configuration of Figure 15 is in reasonable agreement with these results. A closer agreement can be envisioned when the effect of the relatively large size of the retro-reflector compared to an ideal point source is considered. Also the retro-reflector was not within the Fraunhofer or far field region of the optics.

By observing the chopped retro-return signal while the retro-reflector position was moved, it appeared as though the detector size was the primary field of view limiting factor. As the target is moved in the object plane, the Airy disk moves proportionately in the focal plane. For a small detector, a small movement in the object plane will cause the focused signal to depart from the active detector area and detection ceases. The relationship describing this situation is

$$\theta = \frac{x}{f}$$

where x is the detector diameter and f is the optics focal length. For both optical configurations, the detector

diameter was approximately seven mils. For the optical configuration of Figure 15, the field of view predicted by this relationship is 116 μ radian, and for the optical configuration of Figure 14, the field of view is predicted as 875 μ radian. Both of these predicted results remain considerably smaller than the observed results. Again, however, this prediction is predicated upon the target being in the optics far field. It also assumes the signal energy to be confined within the Airy disk. Due to the considerably increased sensitivity of heterodyne detection, the system should easily be capable of detecting energy well out into the diffraction ring area. This may be the cause of the larger than predicted field of view.

5. Transmitter Divergence

In a laser radar system the transmitted beam divergence is the counterpart of the microwave radar's transmitter antenna gain. It must be fairly accurately known before any meaningful system performance calculations can be made. If the transmitted and received powers and target and receiver apertures are known, the beam divergence can be easily computed. The divergence calculations were made with the optical configuration of Figure 15. The retro-reflector was at a range of 305 yards.

The linear arc length of a beam of a given divergence at a range R is

$$d = R\theta \ .$$

The area covered by the beam at this range is

$$A_1 = \pi(\frac{d}{2})^2 = \pi(\frac{R\theta}{2})^2 \ .$$

The portion of the returned energy is the ratio of the area of the retro-reflector to the area of the beam.

$$\text{Returned energy} = \frac{P_t \ \pi \ (\frac{D_t}{2})^2}{\pi \ (\frac{R\theta}{2})^2} \tag{33}$$

If the retro reflector preserves the transmitted divergence (a reasonable assumption), then the received portion of retransmitted energy will be

$$\frac{\pi \ (\frac{D_r}{2})^2}{\pi \ (\frac{R\theta}{2})^2} \ . \tag{34}$$

The value of the received power will be

$$P_r = \frac{P_t \ \pi \ (\frac{D_t}{2})^2 \ \pi \ (\frac{D_r}{2})^2}{\pi \ (\frac{R\theta}{2})^2 \ \pi \ (\frac{R\theta}{2})^2} \ . \tag{35}$$

Solving for θ results in

$$\theta = [\frac{P_t}{P_r} \ \frac{D_t^2 \ D_r^2}{R^4}] \tag{36}$$

Using the below data, a transmitter divergence of 1.71 milliradians was calculated.

P_t = .65 watts

P_r = .75 milliwatts

D_r = 6 inches

D_t = 2 inches

R = 305 yards

The transmitted power was measured with the higher power analog power meter while the received power was measured with the lower power digital power meter. Accurate results were predicated upon the absolute calibration of each of these devices. A calibration error of either device would, of course, be a source of error.

6. Detector Evaluation

Four detectors were used or evaluated during this project. The first detector used was a Raytheon IR-101 PbSnTe photovoltaic detector. It was extremely useful for alignment procedures since it exhibited a high quantum efficiency and was capable of detecting powers up to 200 mw. It was packaged in a glass dewar, however, and as such was extremely vulnerable to external RFI. This proved to be a considerable problem. Also the frequency response of the detector was below the required value of 35-45 MHz. To achieve a reasonable system S/N level, the modulator had to be operated at a frequency below the desired linear region of 35-45 MHz.

The second detector used was a Rockwell International 5-128-4 PbSnTe photovoltaic detector. Its frequency response was well beyond the required value, and although the quantum efficiency appeared to be lower than several of the other detectors, its system performance exceeded all others. The received S/N ratio as a function of detector bias was recorded for the optical configuration of Figure 14. As can be seen by Table 3, a reverse bias beyond .2 volts results in no further received S/N ratio.

The next detector evaluated was a Rockwell International 7-229A. This detector exhibited a quantum efficiency approximately twice that of the other Rockwell detector, but the frequency response was again a problem. A reverse bias of .075-.6 volts was applied, but this was not sufficient to raise the frequency response to the required level. With the system frequencies lowered to 27-36 MHz, the best attainable S/N was 5 db below the Rockwell 5-128-4 detector.

The last detector evaluated was an Aerojet General PbSnTe, heterojunction, photovoltaic detector. It was a high-impedance detector designed primarily for passive system applications. Although the quantum efficiency appeared reasonably high, the frequency response was much too low to achieve heterodyne detection at the 35-45 MHz region. A reverse bias of .075-.5 volts was applied; however, no heterodyne detection was observed.

7. Receiver Sensitivity

The measure of the receiver sensitivity of a radio-frequency radar is usually termed the minimum discernible signal or MDS. For optical systems, however, this parameter is more commonly expressed as the noise equivalent power or NEP. It is defined as the signal power necessary to produce a signal-to-noise ratio of unity. This can be easily computed if the received power, effective noise bandwidth, and measured system S/N ratio are known. The actual received power incident upon the detector could not be directly measured, but an estimation was obtained from the measured receive power prior to the 5/95 splitter and a knowledge of the optical parameters.

The Airy disk diameter for a far field target can be computed by

$$d = 2.44\ \lambda\ (f/no)_{eff} \tag{37}$$

where the effective (f/no) for a Newtonian antenna was computed from [Ref. 9]

$$(f/no)_{eff} = \frac{f}{D_p}\left[\frac{1}{1 - (D_{OBS}/D_p)^2}\right]^{1/2} \tag{38}$$

For this relationship f is the focal length of the primary mirror, D_p is the diameter of the primary mirror and D_{OBS} is the diameter of the obstructing mirror. The diameter of the detector used was known to be approximately 8 mils.

The detector, therefore, was estimated to be 75% of the Airy disk diameter. From the energy density profile of the Airy disk [Ref. 4], it was estimated that approximately 80% of the energy within the Airy disk was incident upon the detector. Of the total incident energy approximately 84% of the energy is contained within the Airy disk [Ref. 9]. The dewar window transmittance was estimated to be approximately .8. The far field of a lens system can be computed from [Ref. 9]

$$x = \frac{D^2}{2\lambda} \tag{39}$$

where D is the lens aperture diameter. The far field of the optical configuration of Figure 15 was computed to be 1001 yards. With the retro-reflector at 305 yards, the effective object range was 610 yards. It was assumed that the difference between this range and the antenna's far field would have little effect upon the computed Airy disk size.

Using the above relationships and the experimental conditions listed below, the system NEP for the optical configuration of Figure 15 was calculated to be

$$\frac{NEP}{B} = \frac{S}{(S/N)B} = \frac{3.8\times10^{-4}\text{Watts}}{(10^6)(5\times10^4\text{Hz})} = 7.6\times10^{-15}\text{Watts/Hz} \tag{40}$$

Total Spectrum S/N	55 db
Range Frequency S/N	60 db
Transmitted Power	.65 w

Returned Signal Power	.71 mw
Chopped Signal Output	5.5 mv
Chopped L.O. Output	1.4 mv

The returned signal power for the optical configuration of Figure 14 was too low to be measured with the available power measuring equipments. Using the transmitted power, target distance, beam divergence, and effective receiver aperture, the signal power was computed to be 7.53×10^{-6} watts from the following relationship:

$$P_r = \frac{P_t \, \pi \, (\frac{D_t}{2})^2 \, \frac{\pi ab}{4} \, .45}{(\frac{R\theta}{2})^4 \, \pi^2} \quad . \tag{41}$$

The factor $\frac{\pi ab}{4}$ is the effective receiver aperture. It is the area of an ellipse with major and minor axes a and b, respectively. The elliptical area is a result of the beamsplitter's subtending a 45° angle to the received wavefront. The factor .45 accounts for the two 5/95 and the 50/50 splitters within the receive path. Using the data listed below, the system NEP was calculated to be

$$\frac{NEP}{B} = \frac{7.53 \times 10^{-6} \text{Watts}}{(5 \times 10^{6})(5 \times 10^{4} \text{Hz})} = 3.01 \times 10^{-17} \text{Watts/Hz}$$

Range Frequency S/N	67 db
Transmitted Power	.23 w

Returned Signal Power (Calculated)	7.53×10^{-6} w
Local Oscillator Power	3 mw

From equation (9) it can be seen that for shot noise limited heterodyne detection, the theoretical limit of NEP is

$$\frac{NEP}{B} = 1.88 \times 10^{-20} \text{Watts/Hz} \ .$$

The previously measured value of η by the Rockwell International Science Center was .32 [Ref. 37]; therefore, the theoretical limit of NEP for the detector used was

$$NEP = 5.86 \times 10^{-20} \text{Watts/Hz} \ .$$

Therefore, it can be seen that the best attainable system performance resulted in approximately three orders of magnitude below the theoretical limit. The local oscillator power of 3 mw for the optical configuration of Figure 14 should have been sufficient to produce shot noise limited operation. Shot noise limited operation can be easily verified by observing the background receiver noise as the local oscillator power is increased. No such increase was observed for either optical configuration. The theoretical power required for shot noise limited operation can be computed from [Ref. 2].

$$\frac{NEP}{B} = \frac{h\nu}{\eta} \left[1 + \frac{2K\,(T_m + T'_{IF})\,G_D}{q} \left(\frac{h\nu}{\eta q P_{LO}}\right)\right] \qquad (42)$$

where T_m is the physical detector temperature, T'_{IF} is the amplifier effective noise temperature, and G_D is the detector conductance.

For the system investigated, $G_D = \frac{1}{50\Omega}$, $\eta = .32$, $T_m = 77°K$ and $T'_{IF} \approx 870°K$ (a generous estimate) which corresponds to an amplifier noise figure of 6 db.

For shot noise limited operation, the first term of (42) must predominate the equation which requires

$$\frac{h\nu}{\eta} << 2K\ (T_m + T'_{IF})\ G_D\ (\frac{h\nu}{\eta q})^2\ \frac{1}{P_{LO}}$$

or

$$P_{LO} >> 2K\ (T_m + T'_{IF})\ G_D\ (\frac{h\nu}{\eta q}) \qquad (43)$$

Using the specified system parameters given above, the required value of P_{LO} must be $P_{LO} >> .42$ mw. Thus it can be seen that a local oscillator power of 3 mw should induce enough shot noise power to dominate other noise sources

With a S/N ratio of 60 db registered from the retro-reflector at 305 yards, a diffuse reflector was placed immediately in front of the reflector. No signal return could be observed from the diffuse reflector. The diffuse reflector consisted of a three-inch by six-inch piece of sand-blasted aluminum. If the diffuse reflector were a perfect Lambertian surface, the returned signal irradiance (H) can be computed from

$$H = \frac{WA_D}{\pi R^2} \tag{44}$$

where WA_D is the diffuse reflector power returned and is expressed by the relationship

$$WA_D = \frac{P_t A_D}{\pi (\frac{R\theta}{2})^2} \tag{45}$$

where W is the radiant intensity and is the power density returned per unit area of the reflector.

From these relationships it can be seen that

$$P_r = \frac{P_t A_D A_r}{\pi (\frac{R\theta}{2})\ \pi R^2} \tag{46}$$

where A_D is the area of the diffuse reflector, and A_r is the effective receiver aperture.

Comparing this result with equation (35), it can be seen that a reduction of 53.8 db could be expected from a perfect Lambertian reflector of the size used. If the reflection coefficient of the sandblasted diffuse target is considered to be .79 [Ref. 9], then an additional reduction of 1 db would result. If the reflection coefficient were as low as .1 due to oxidation, then the additional decrease could be as much as 10 db. The actual reflection coefficient encountered was expected to lie somewhere in this mentioned range. An additional degradation of the

signal level was a masking effect caused by the strong local oscillator contaminating signal. This signal could easily have masked the small expected return from the diffuse reflector.

VII. CONCLUSIONS AND RECOMMENDATIONS

A. CONCLUSIONS

The receiver sensitivities achieved were quite disappointing. If the theoretical limit had been achieved, an approximate sensitivity increase of 30 db would have been realized with the optical configuration of Figure 14. Also, if the optical configuration of Figure 15 had realized the theoretical S/N improvement of approximately 15 db over that of Figure 14, its theoretical performance should have been about 112 db S/N. With this degree of system sensitivity, a three-inch by six-inch diffuse target should be observable at a range of approximately 2500 yards. It is doubtful that this degree of performance would be acceptable for a search, tracking or threat warning system for a Naval environment. It was suspected that a portion of the less than expected receiver sensitivity problem was caused by noise introduced by the signal processing electronics. Better filtering and lower noise amplifiers within the processing area should improve the obtainable system S/N. The system sensitivity is an inverse function of the receiver effective noise bandwidth. If this bandwidth were reduced considerably, the over-all system sensitivity could be appreciably increased. The processed signal bandwidth was also larger than desirable. This could have been caused by frequency non-linearity of the modulator driver or

instabilities of the laser. Before the receiver noise bandwidth can be reduced, the processed signal bandwidth must be reduced accordingly.

From the range and velocity measurements, it was clearly evident that the developmental system was capable of simultaneous range and velocity measurements. The velocity resolution measurements were quite impressive. The developmental system would have been capable of detecting several targets simultaneously providing the ranges or velocities were appreciably different. The extremely narrow receiver field of view would limit the system detection to a single or a few targets.

B. AREAS OF POSSIBLE IMPROVEMENT AND FURTHER STUDY

From the receiver 3 db field of view and transmitter divergence measurements, it was obvious that the transmitted energy was inefficiently utilized. A better approach would have been to use separate receive and transmit optics with the transmitter divergence more nearly corresponding to the receiver's effective field of view. A beam expander within the transmitter optics could easily perform this function. The local oscillator contaminating signal prevented close range measurements; therefore, its generation mechanism should be investigated and suppressed. Although this effect was suppressed with the combination of a quarter-wave plate and a wire-grid polarizer, the transmitter power was also reduced by more than 3 db. By eliminating

this effect through its generation mechanism, a larger transmitted power can be achieved. Once this generation mechanism is clearly understood, it is conceivable that it could be optimized and utilized for a variety of system applications. As an example, it could possibly be utilized for a short-range data link type communication system. The full signal processing advantage of a coherent detection process would be available while the receiver would be greatly simplified since a local oscillator laser would not be necessary. Since sufficient local oscillator power would not be available to produce shot noise limited operation, the system sensitivity would be considerably reduced. The degradations of atmospheric amplitude scintillations could easily be overcome by FM or PM modulation methods. Also, the doppler shift from a rapidly moving receiver or transmitter would not be a problem since the modulated and reference signals would be doppler shifted by the same amount. Also, it is not beyond reason to visualize a radar system similar to the developmental system in which a low power AO modulator is utilized to reflect power back into the cavity of a high-power laser for re-amplification. Such a system could possibly achieve transmitted powers several orders of magnitude above the powers achieved with the developmental system.

A study of alternate methods of signal processing or modulation could be conducted to determine an optimum technique.

Possible digital coding modulation schemes could be used that would not require a high degree of frequency linearity of the modulator.

An automatic range and velocity display system could easily be devised using a digital counter and logic circuits.

Lastly, an automatic tracking system would most likely be required within the optics to accommodate the extremely small receiver field of view and stringent heterodyne detection requirements of the received wavefront.

C. POSSIBLE SYSTEM APPLICATIONS

One of the primary applications of an FM-CW radar would be a precision tracking system capable of near the horizon operation. If the system sensitivity were adequate, this aspect should be easily achievable due to the extremely narrow transmitted beam and receiver field of view. The excellent velocity resolution could easily allow a threat velocity search to be conducted and identified. Also due to the excellent velocity resolution, it is conceivable that target vibrations could be sensed and categorized for target identification.

Another application could be an airborne clear air turbulence indicator. It could provide the turbulence range and velocity information. A correlation of the signal intensity with the measured range could possibly yield information concerning the magnitude of index of

refraction change. This should yield information regarding the degree of turbulence expected.

If the system sensitivity could not be increased to effectively perform the above applications, an optical return augmentation device might be used for cooperative targets. Such an application might be for aircraft landing systems in which it is highly desirable to precisely measure the landing aircraft's velocity, range and descent angle.

TABLE 1

OBSERVED FREQUENCY AS A FUNCTION OF RANGE

Triangular Modulation

Δf = 10 MHz

fm = 10 KHz

OBS FREQ = Observed Frequency

CORR FREQ = Corrected Frequency

COMP FREQ = Computed Frequency

RANGE (FEET)	OBS FREQ (KHz)	CORR FREQ (KHz)	COMP FREQ (KHz)
43	345	15	17.5
67	360	30	27.2
91	367	37	37.0
115	375	45	46.8
139	387.5	57.5	56.3
163	395	65	66.3
187	405	75	76.0
211	415	85	85.8

Average Frequency Error: 1.43 KHz

Average Range Error: 3.5 Feet

TABLE 2

DOPPLER FREQUENCY MEASUREMENTS

Figure 33	Down Doppler Shift
$\frac{1}{v}$	$\approx$ 2.7 sec/m
v	$\approx$ .37 m/sec
Expected Frequency Shift	69.5 KHz
Observed Frequency Shift	80 KHz
Figure 34	Down Doppler Shift
$\frac{1}{v}$	$\approx$ 1.8 sec/m
v	$\approx$ .56 m/sec
Expected Frequency Shift	104 KHz
Observed Frequency Shift	110 KHz
Figure 35	Up Doppler Shift
$\frac{1}{v}$	$\approx$ 1.6 sec/m
v	$\approx$ .63 m/sec
Expected Frequency Shift	117 KHz
Observed Frequency Shift	120 KHz
Figure 36	Up Doppler Shift
$\frac{1}{v}$	$\approx$ 1.7 sec/m
v	$\approx$ .59 m/sec
Expected Frequency Shift	110 KHz
Observed Frequency Shift	115 KHz

TABLE 3

S/N AS A FUNCTION OF DETECTOR BIAS

Optical Configuration of Figure 14

Rockwell International Detector 5-128-4

S/N	Reverse Bias
60 db	.075 v
62 db	.1 v
65 db	.15 v
67 db	.2 v
67 db	.25 v
67 db	.3 v
67 db	.35 v
67 db	.4 v
67 db	.5 v

P_{LO} = 3 mw

Range = 305 Yards

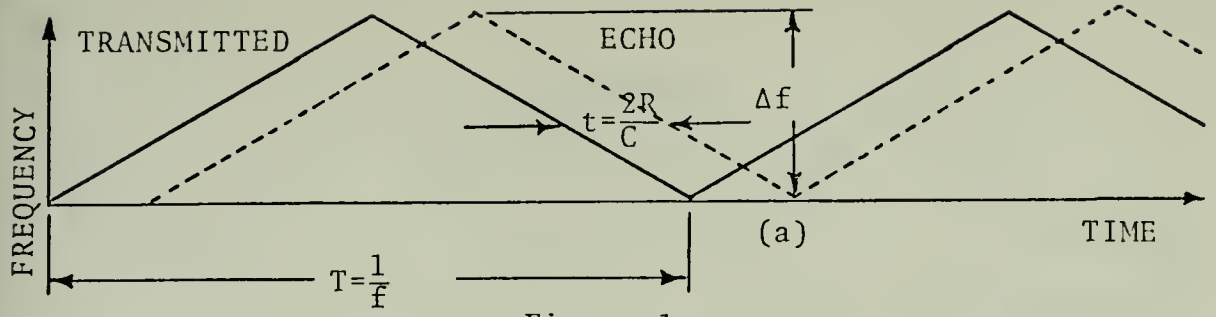

Figure 1.
Linear frequency modulation, stationary target.
(a) Frequency variation of signals.
(b) Observed beat frequency of a single stationary target.

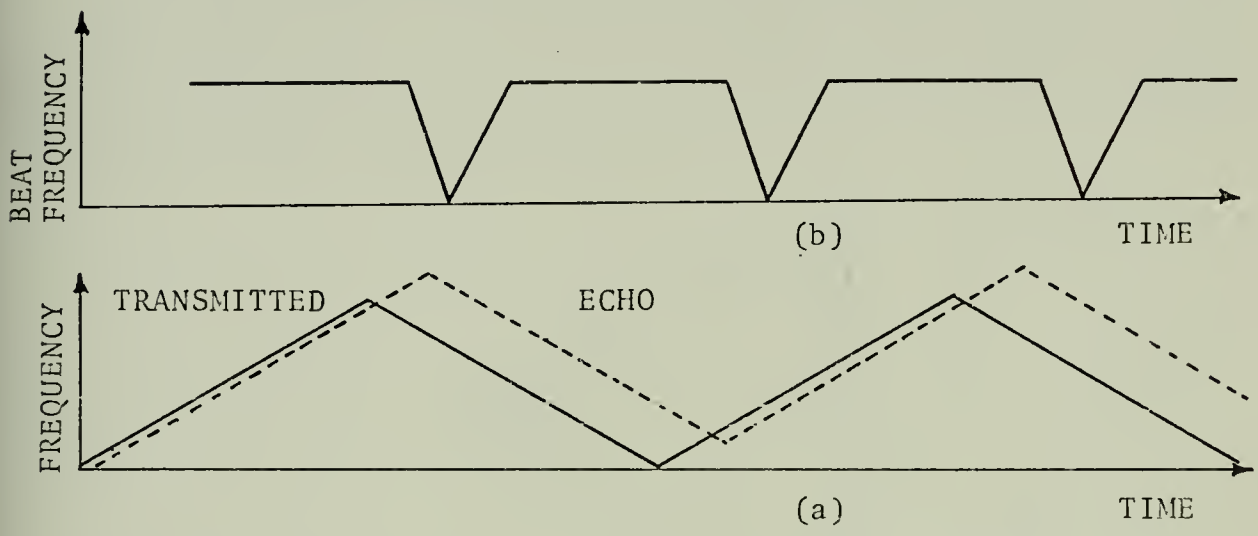

Figure 2.
Linear frequency modulation, moving target.
(a) Frequency variation of signals.
(b) Observed beat frequency of a single moving target.

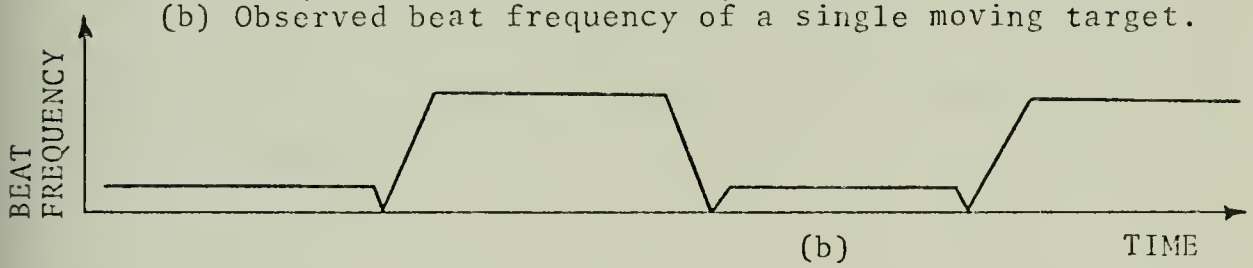

The above figures indicate the relationship between the transmitted and received signals of a linear FM homodyne radar. The resulting beat frequency contains the target's range and velocity information.

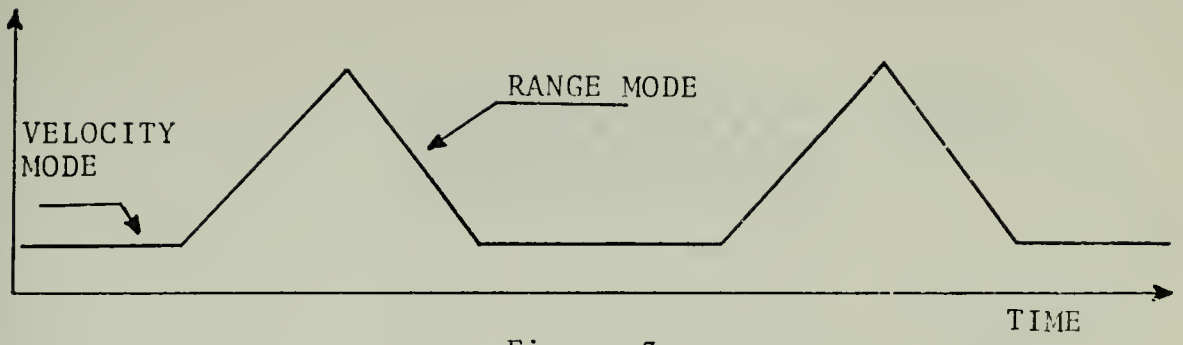

Figure 3.

Dual mode operation of the system.

The CW mode could be used for precision velocity measurement or possible target identification. The FM mode could be used to measure the range information.

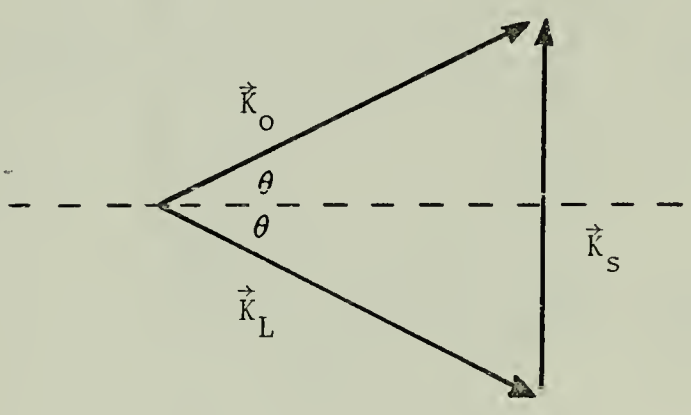

Figure 4.

Incident and resulting wave numbers of the optical and acoustic energies.

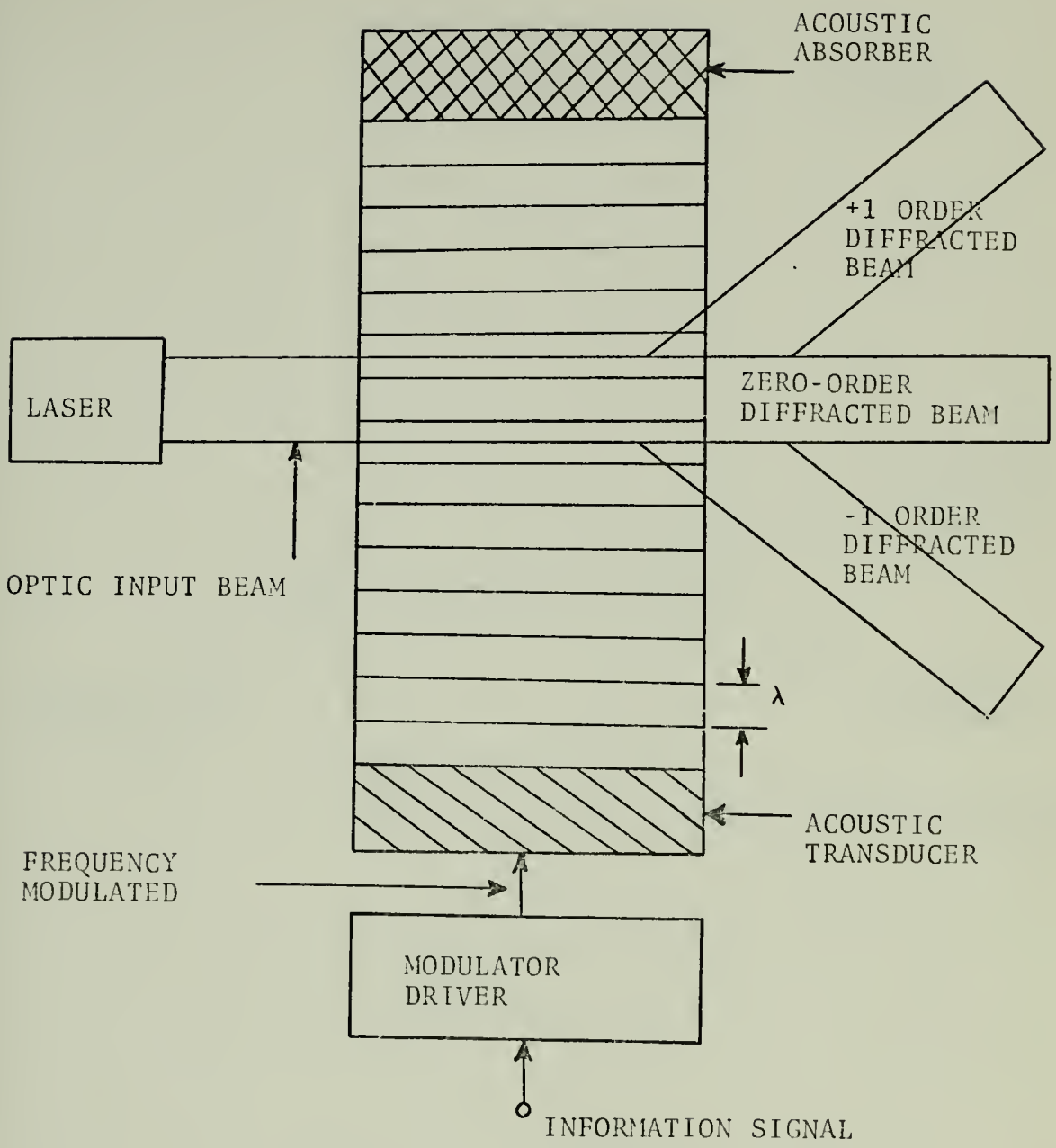

Figure 5.

Basic acousto-optic modulator.

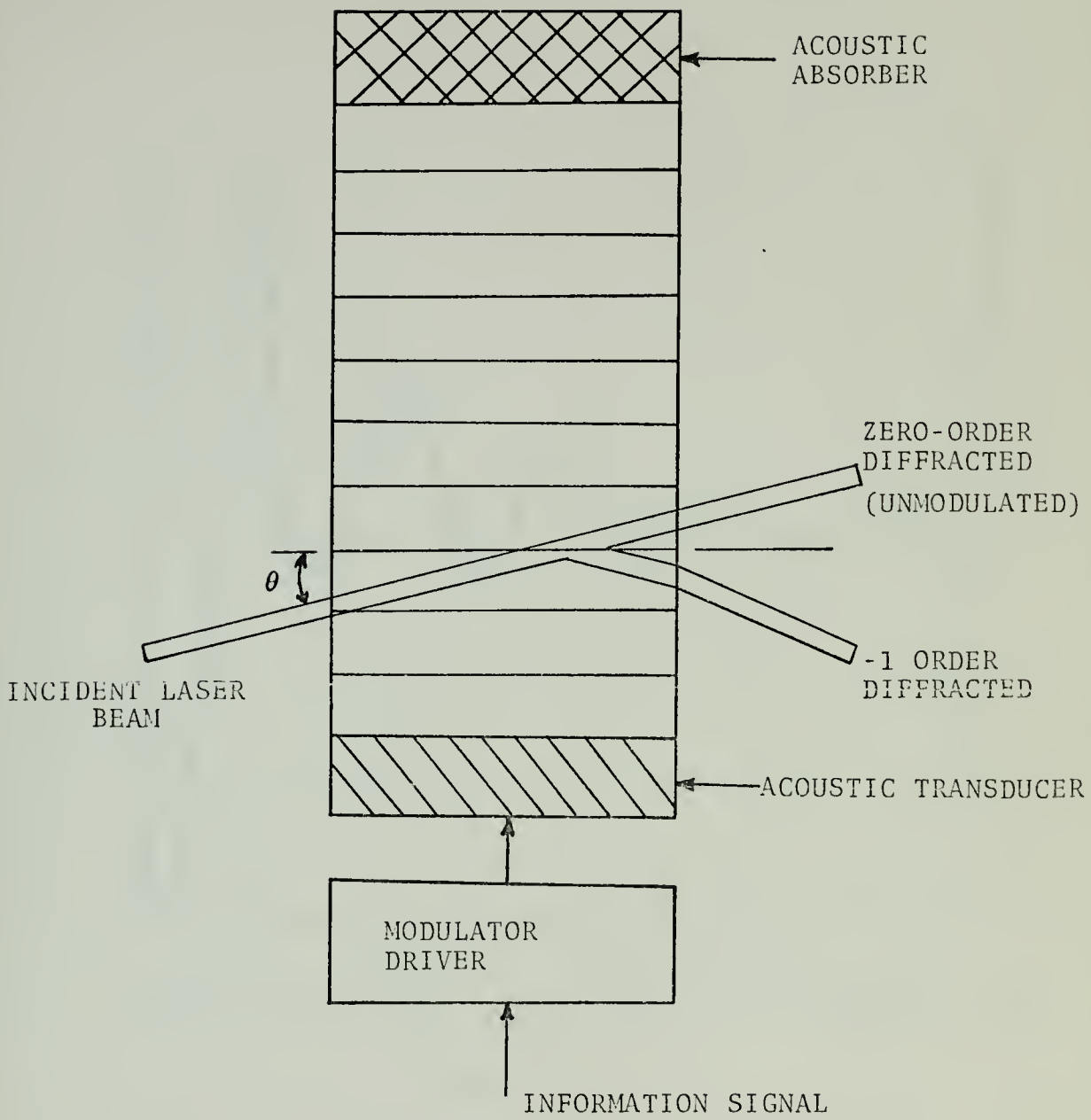

FIGURE 6

Bragg angle acousto-optic modulator.

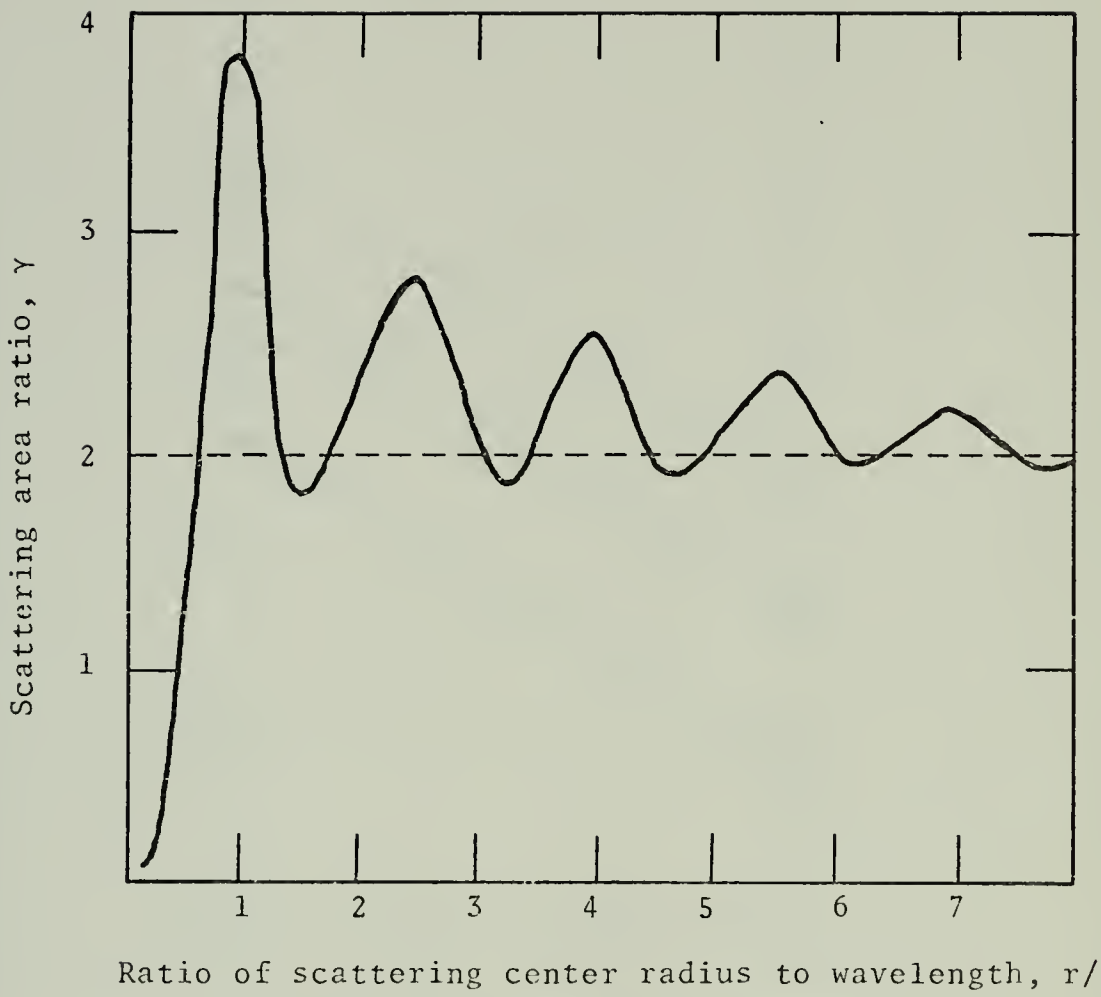

Figure 7.

Scattering area ratio after spherical water drops (Mie scattering).

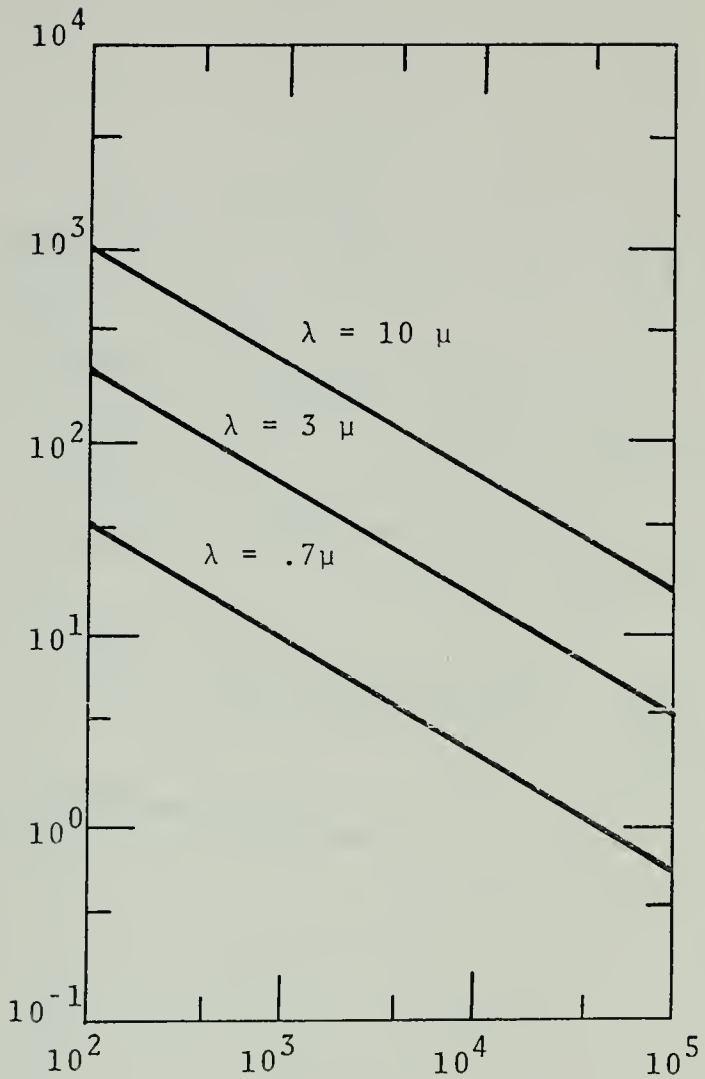

Figure 8.

Lateral phase coherence length for intermediate turbulence.

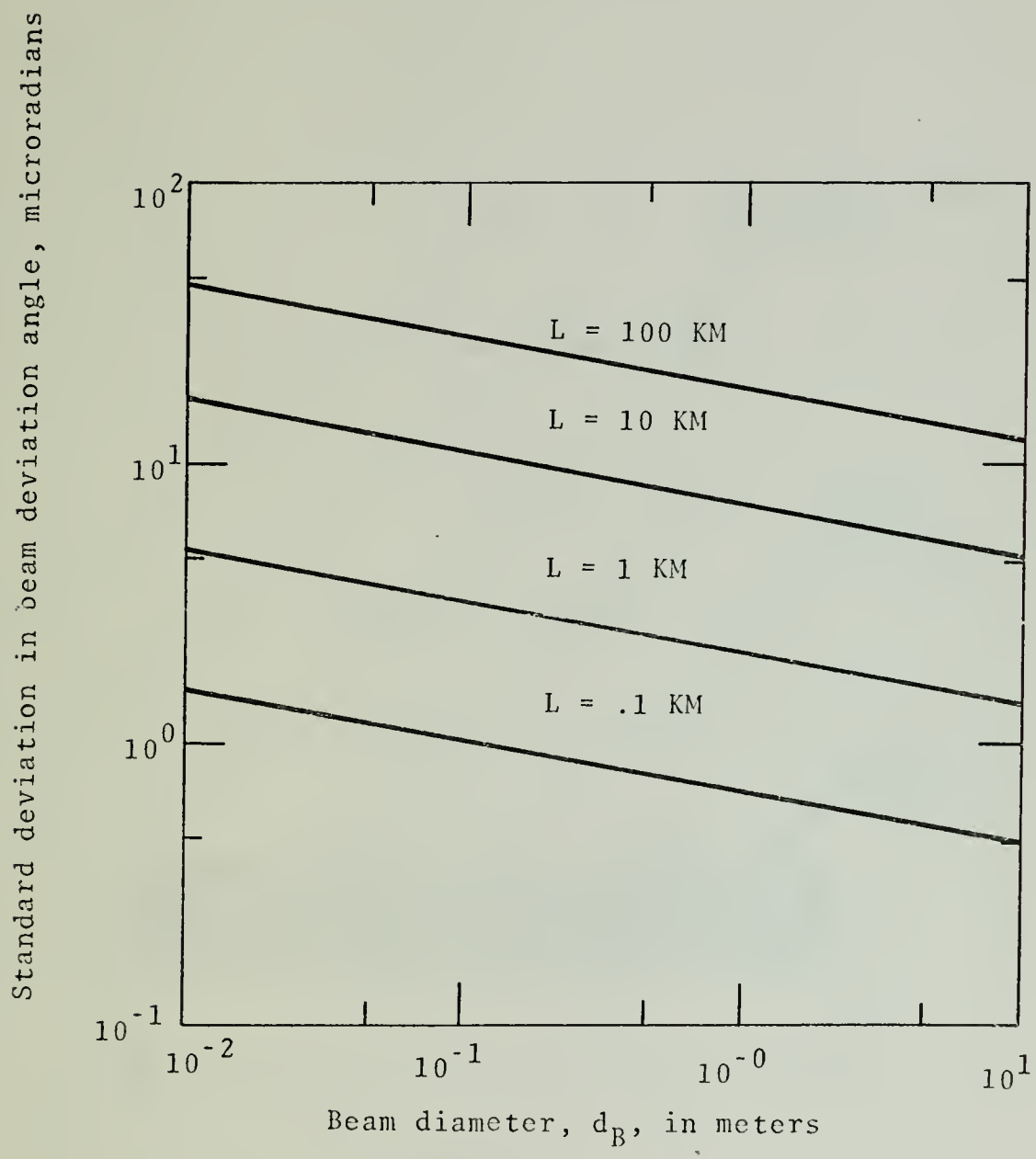

Figure 9.

Standard deviation in beam arrival angle due to intermediate atmospheric turbulence.

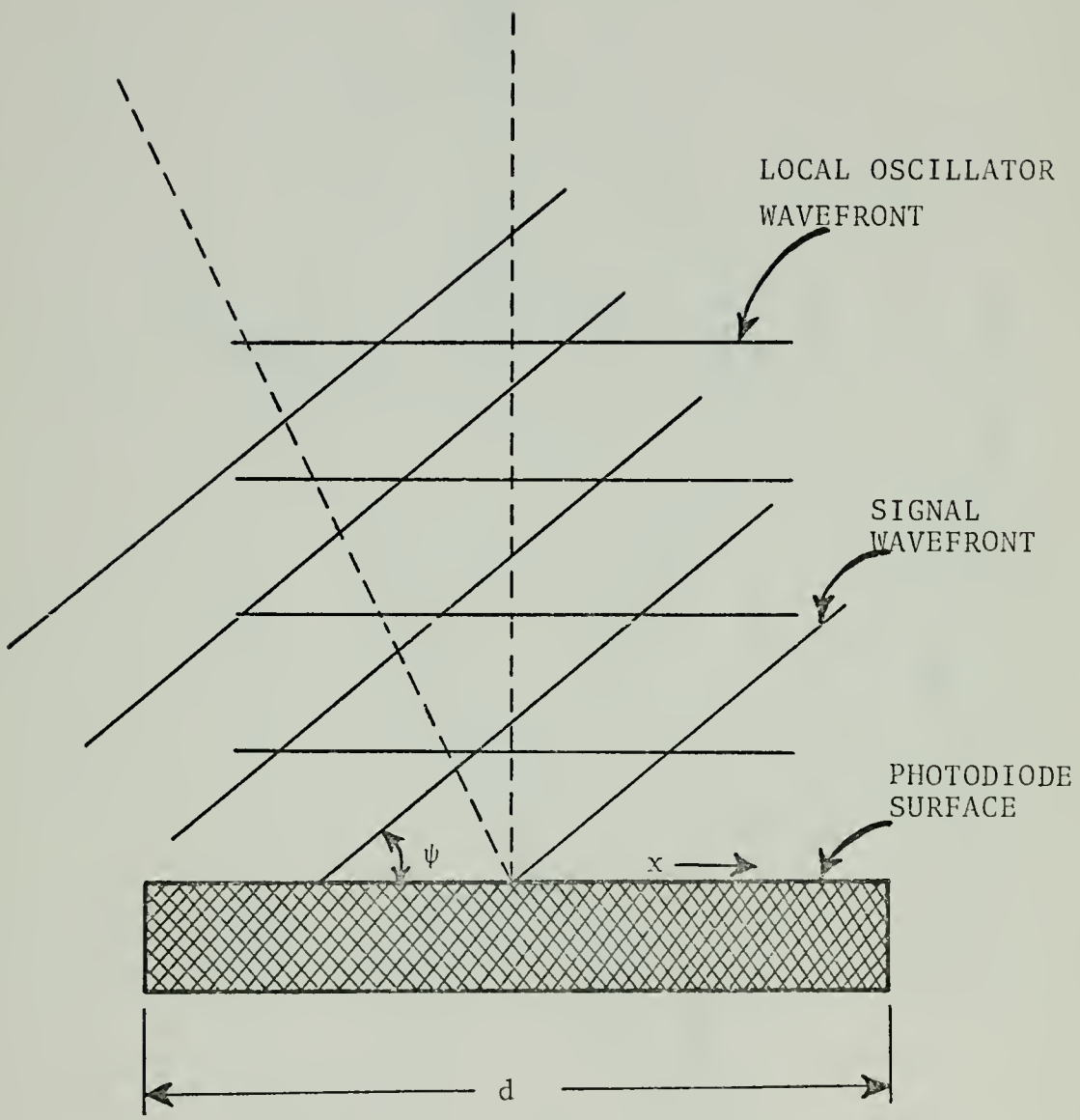

Figure 10.

Spatial misalignment of local oscillator and signal beams

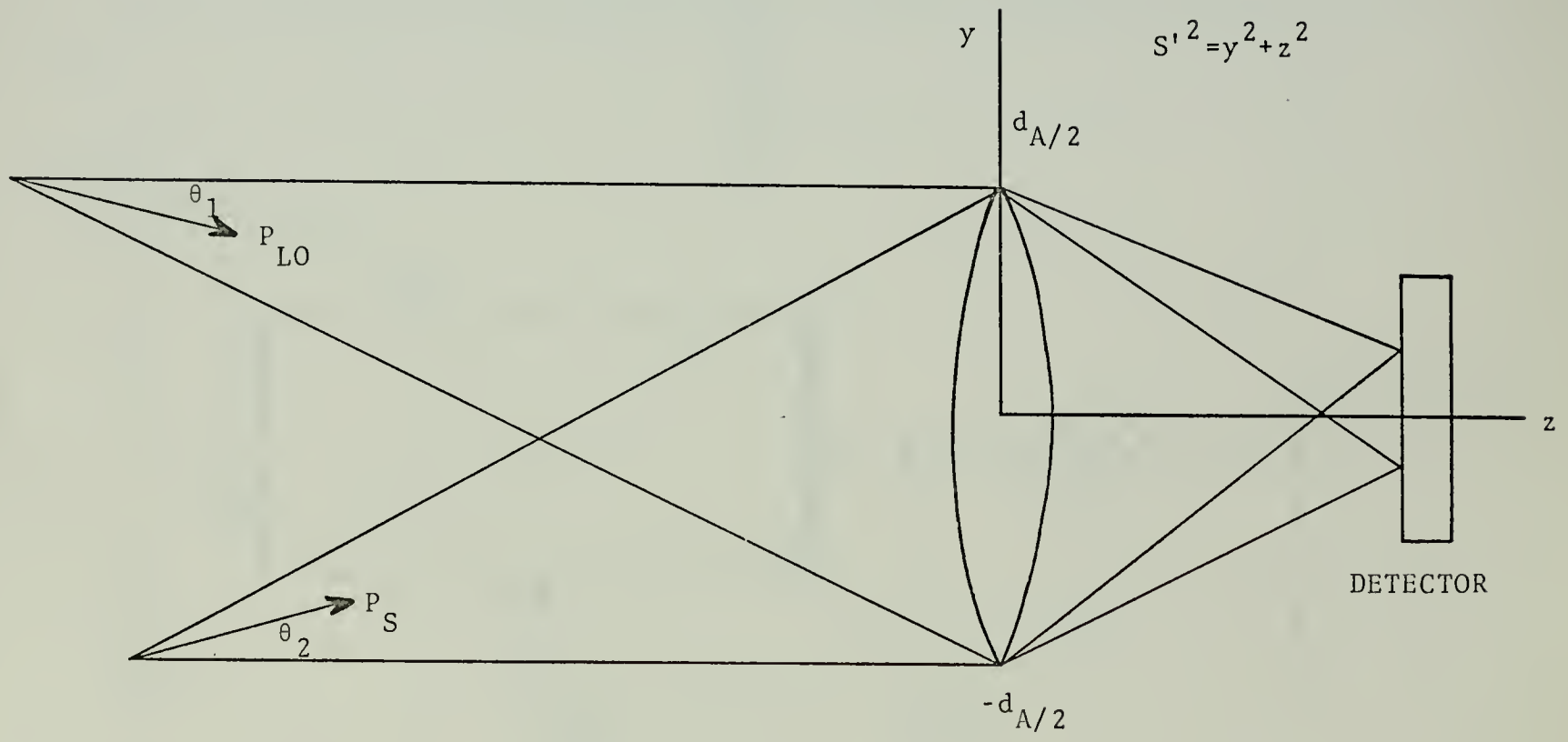

Figure 11.

Heterodyne Detection with Focused Beams.

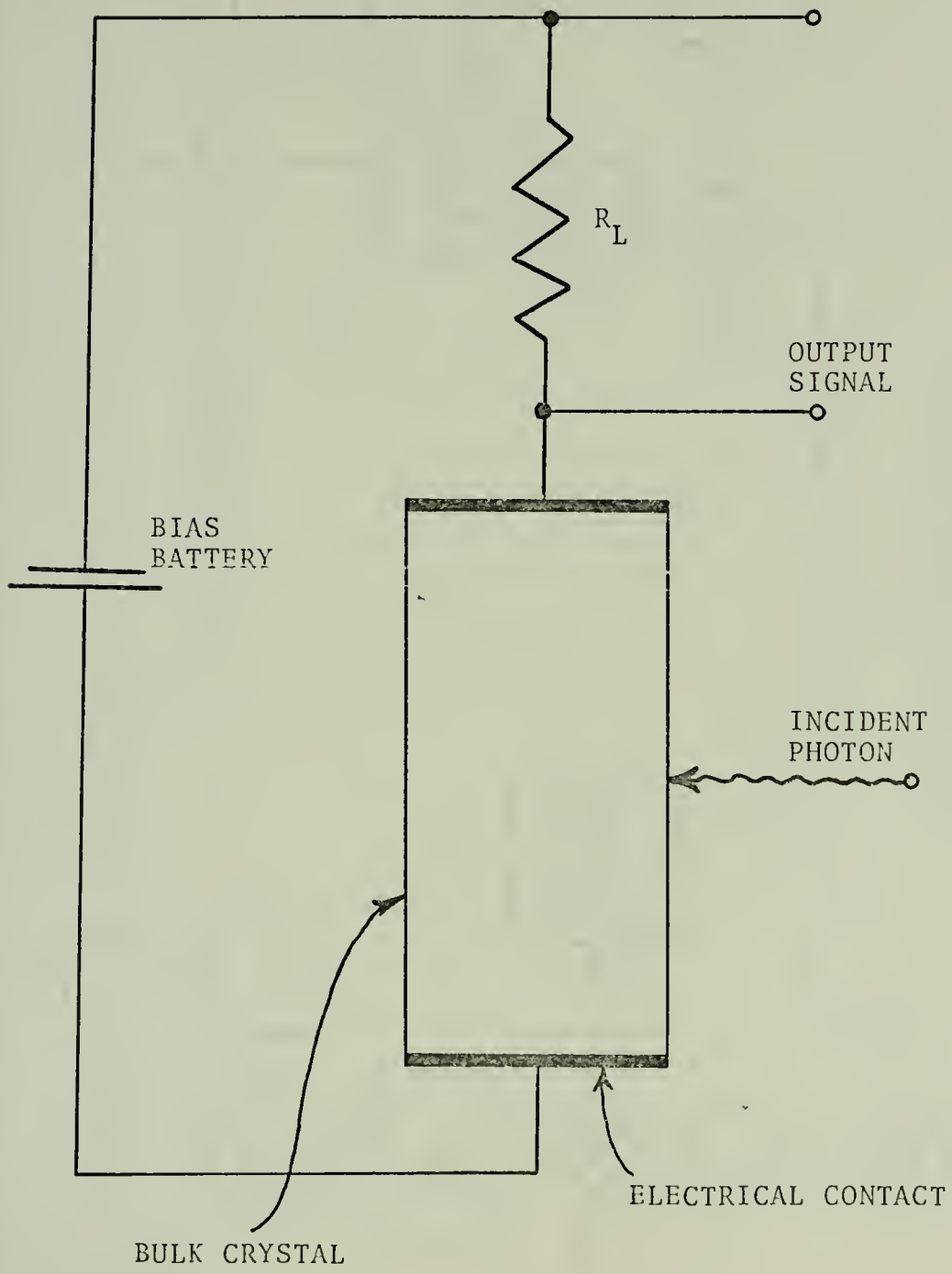

Figure 12.
Simple Photoconductor Circuit.

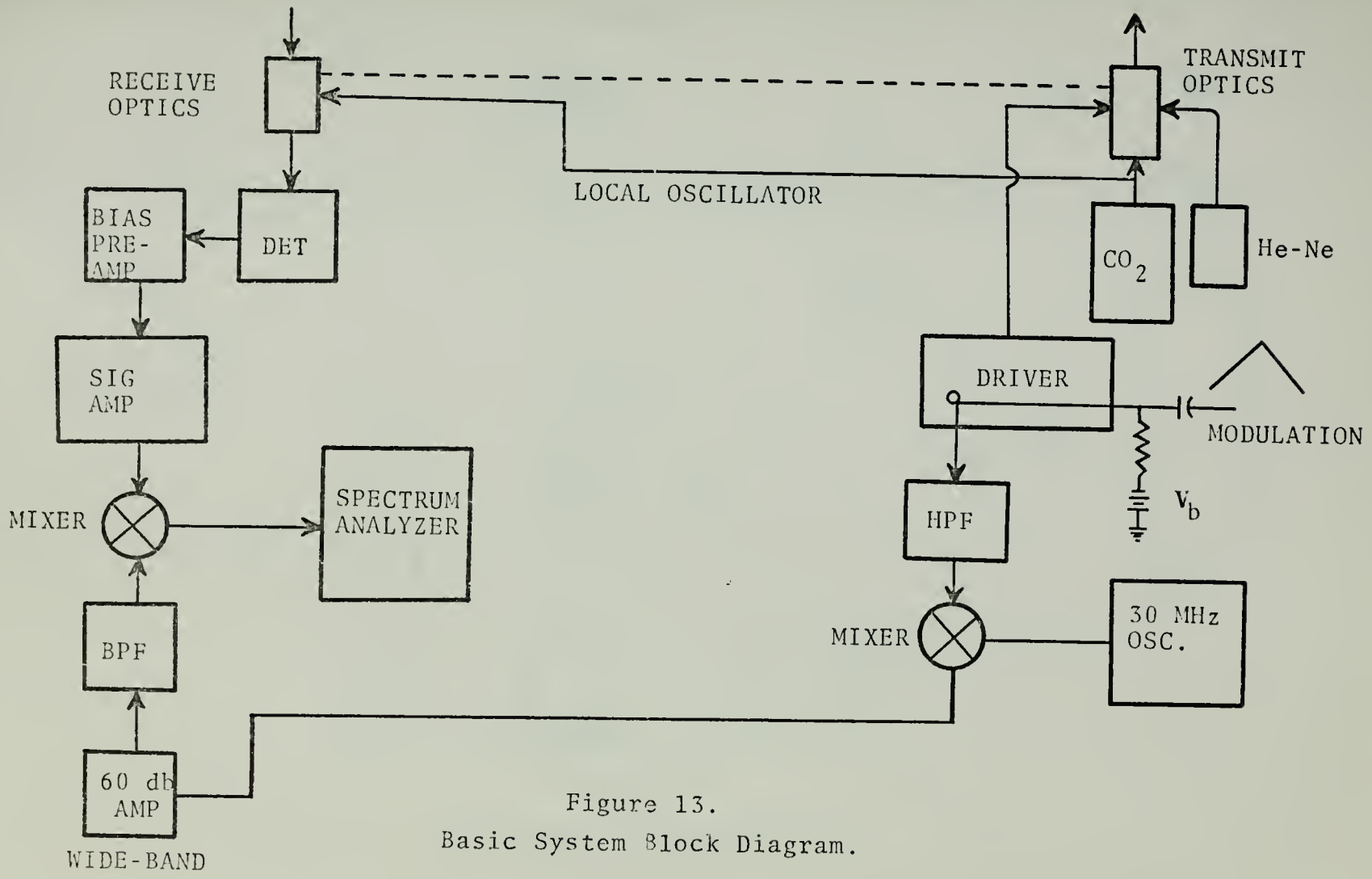

Figure 13.
Basic System Block Diagram.

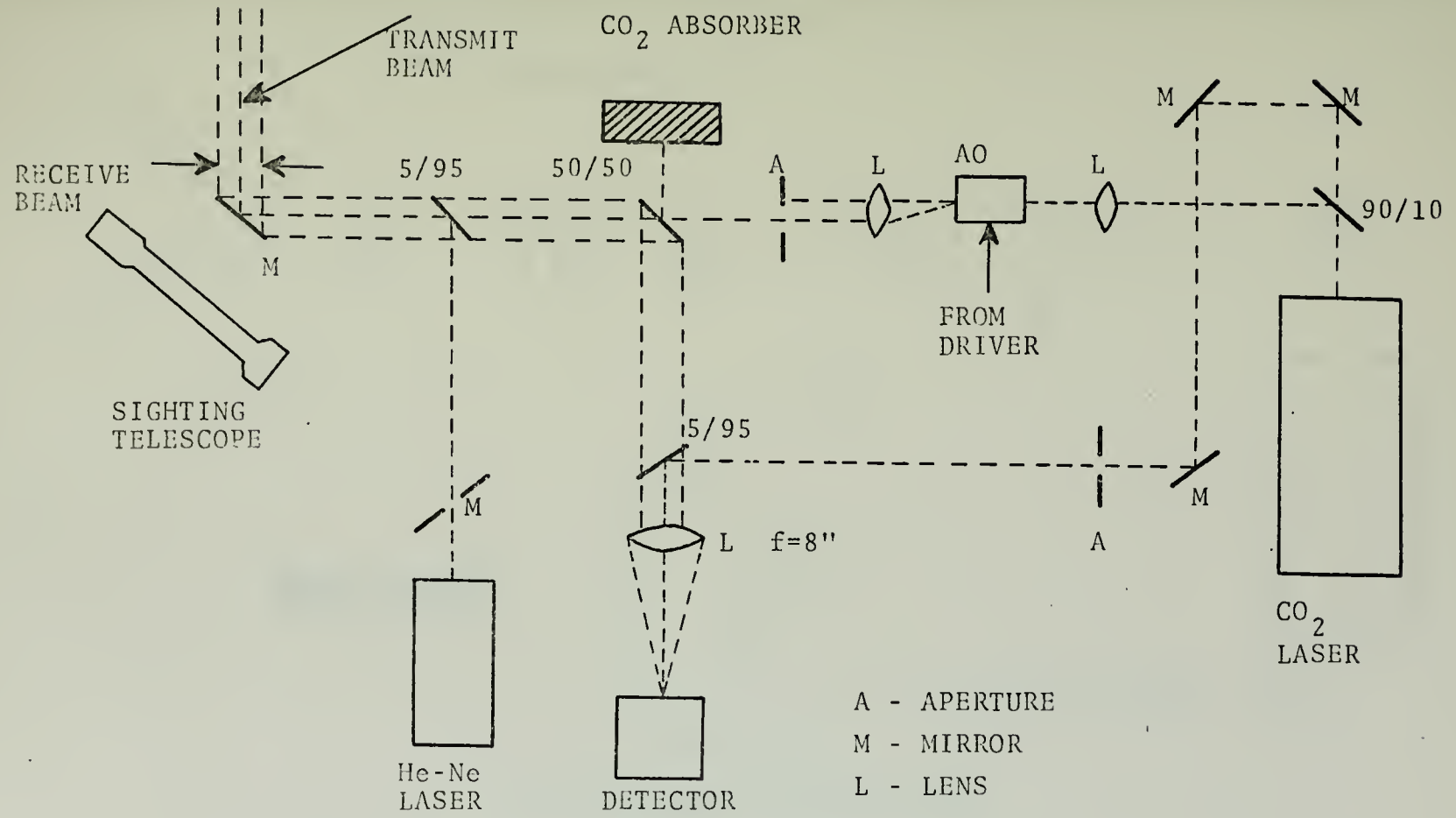

Figure 14.

First Optical Configuration.

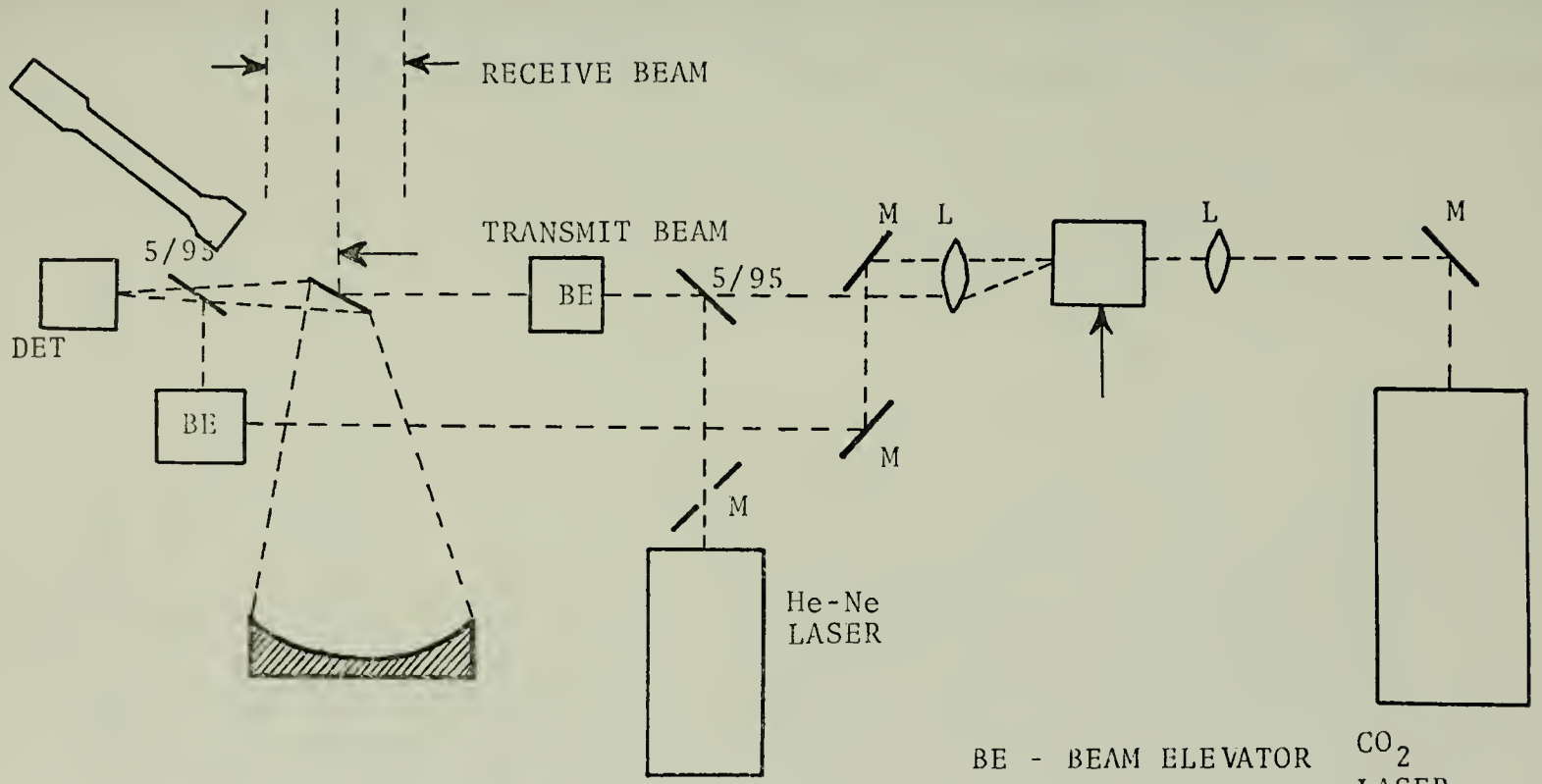

Figure 15.

Second Optical Configuration.

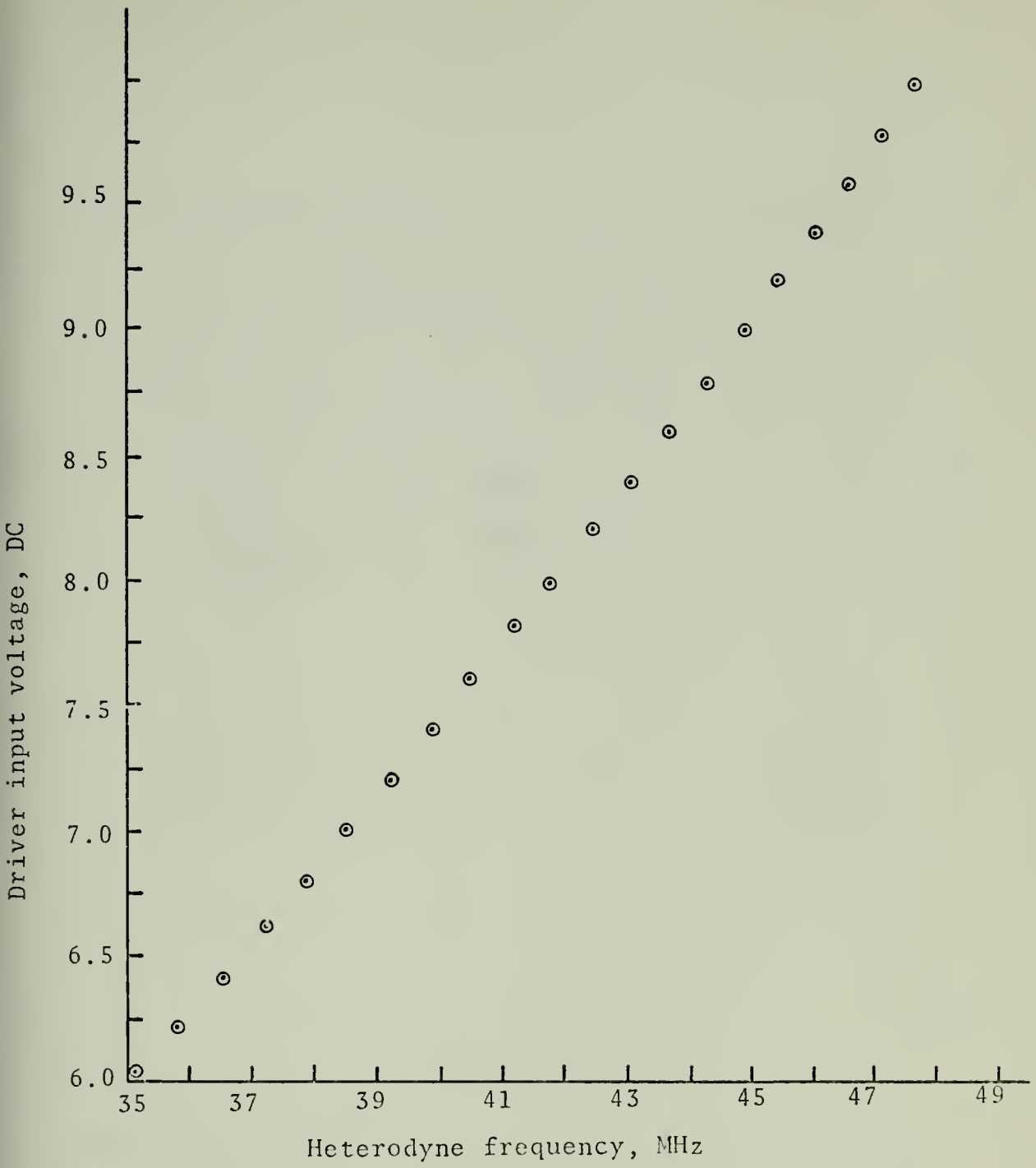

Figure 16.

Modulator frequency linearity.

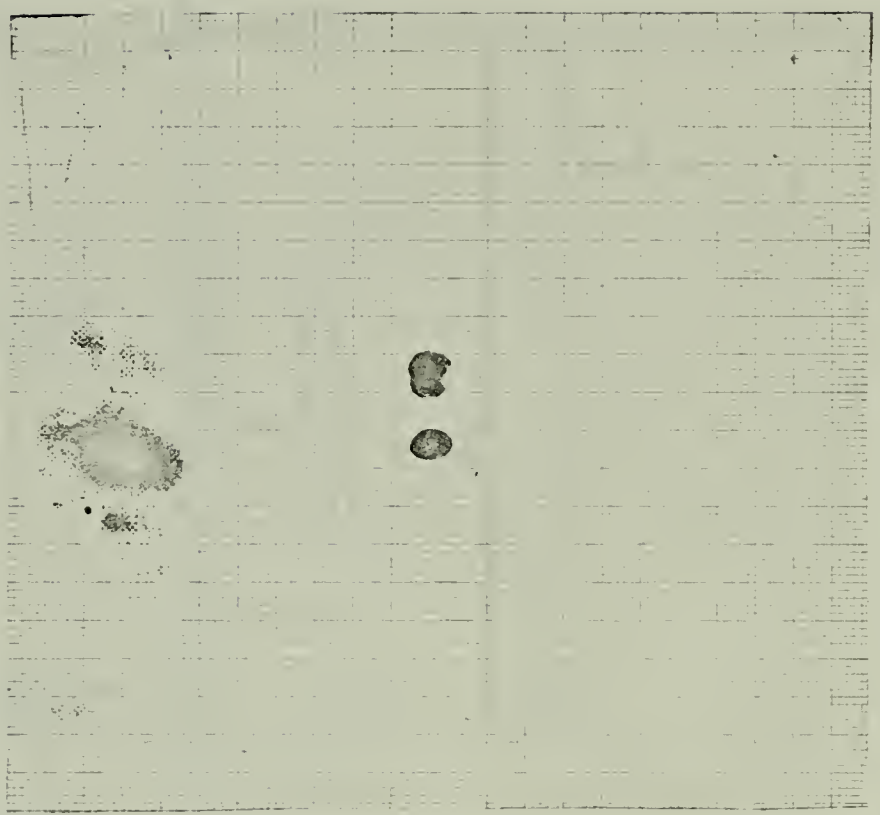

Figure 17.

Spatial intensity recording of modulated and zero-order diffracted beams. Recording was taken after the modulator colimating lens.

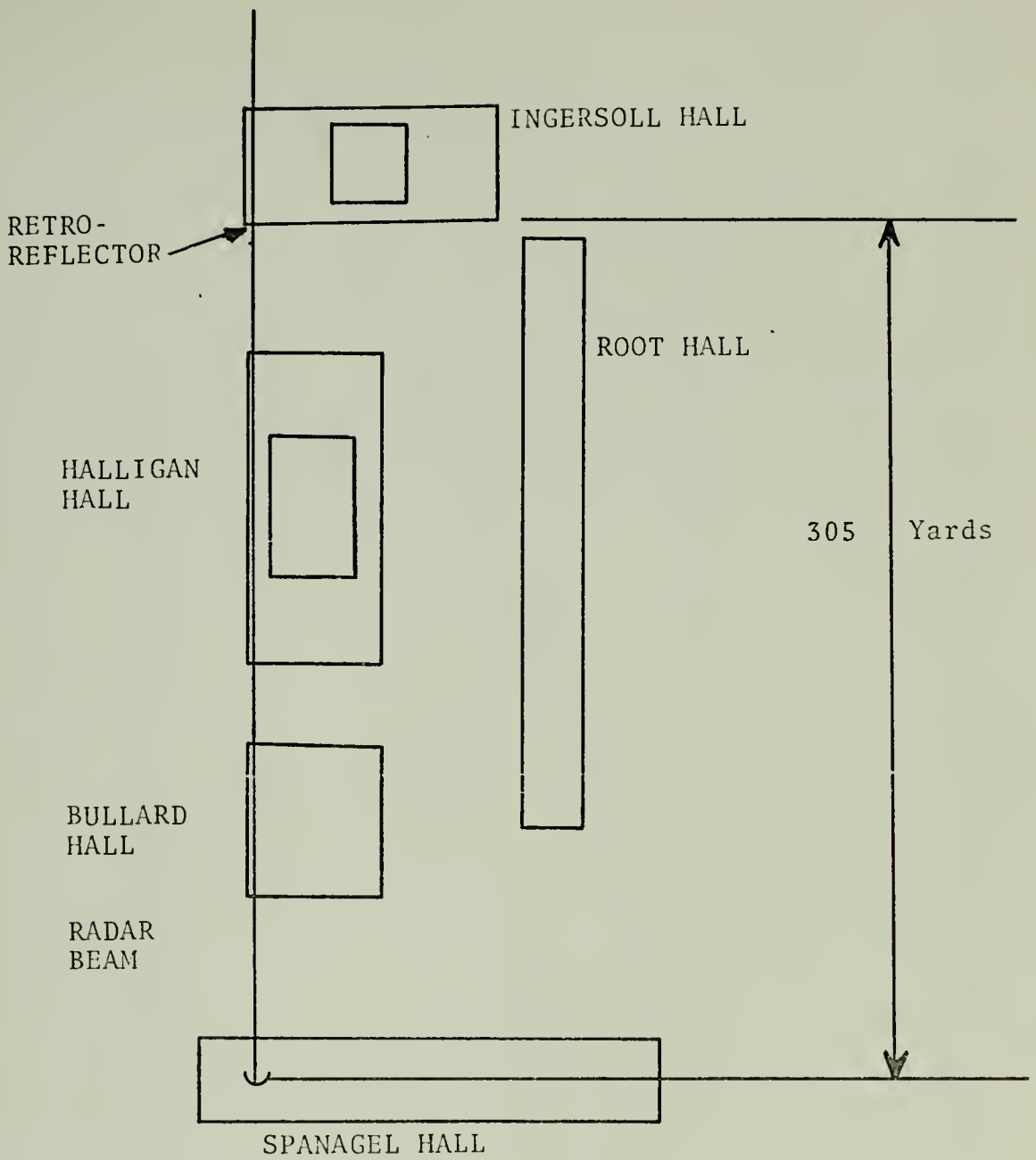

Figure 18.

Map of NPS.

Figure 19
Observed beat frequency as a function of range.

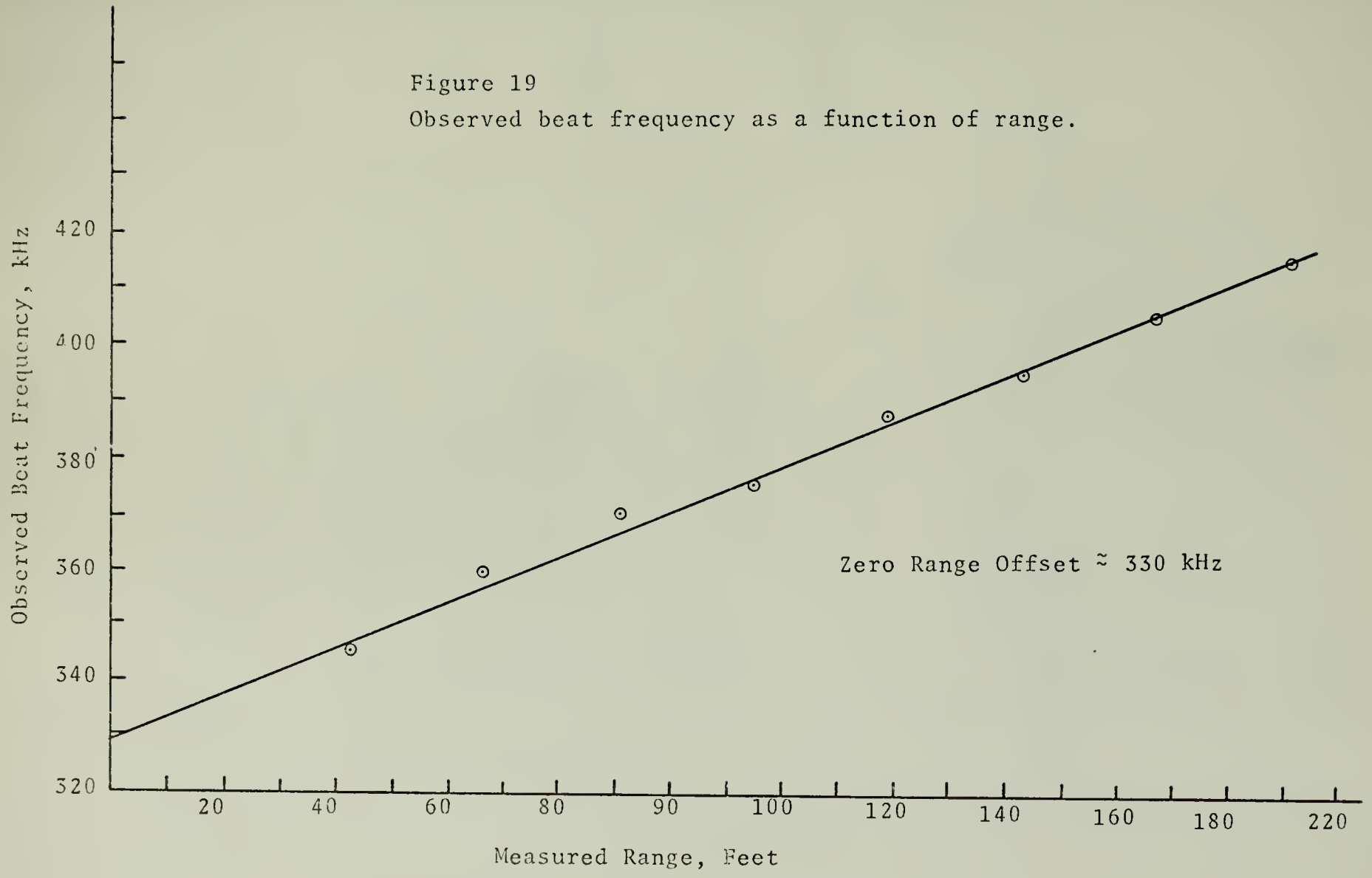

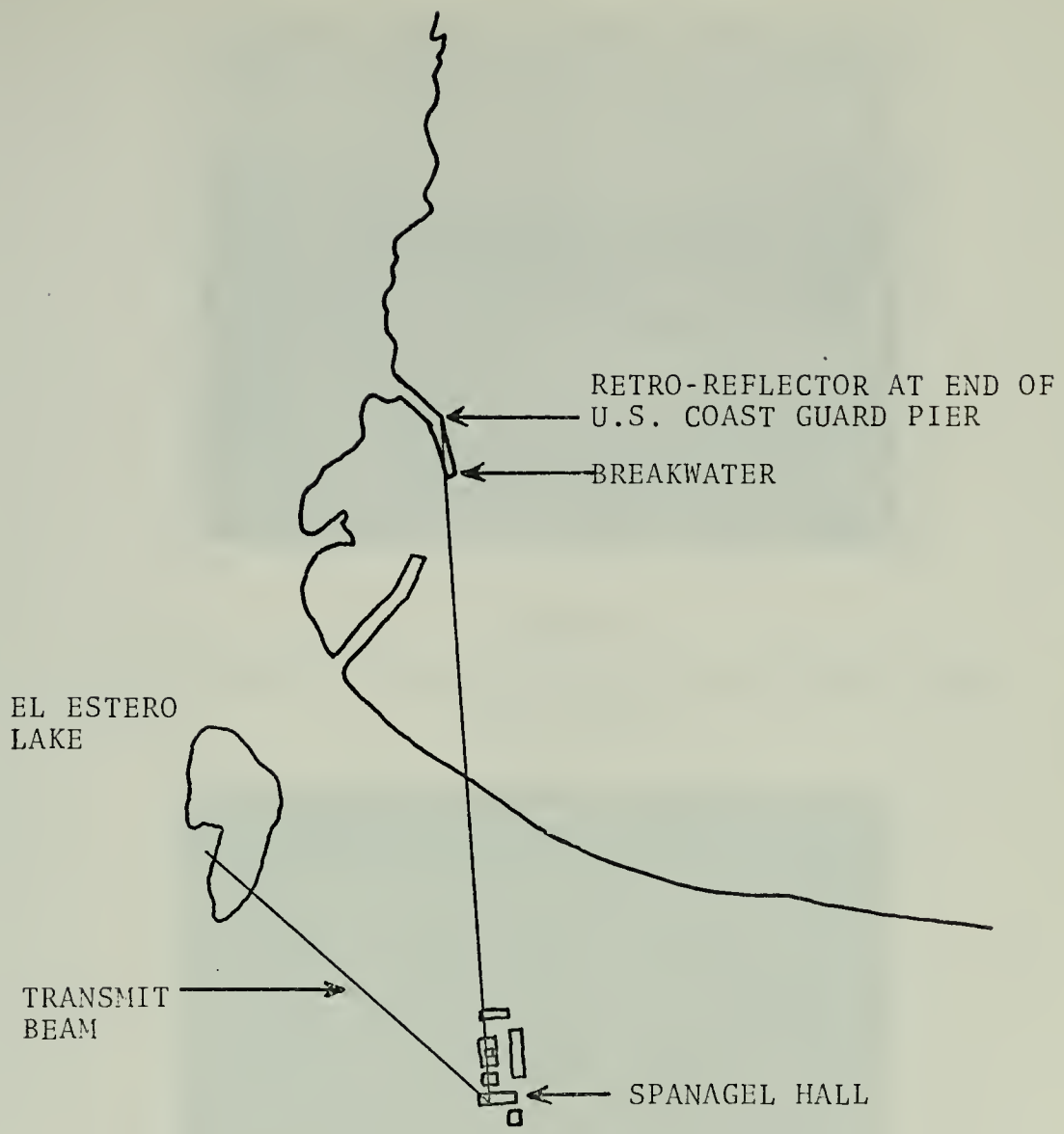

Figure 20.

Map of Local Area.

Figure 21.
Photograph of beam path used for 305 yard range measurements.

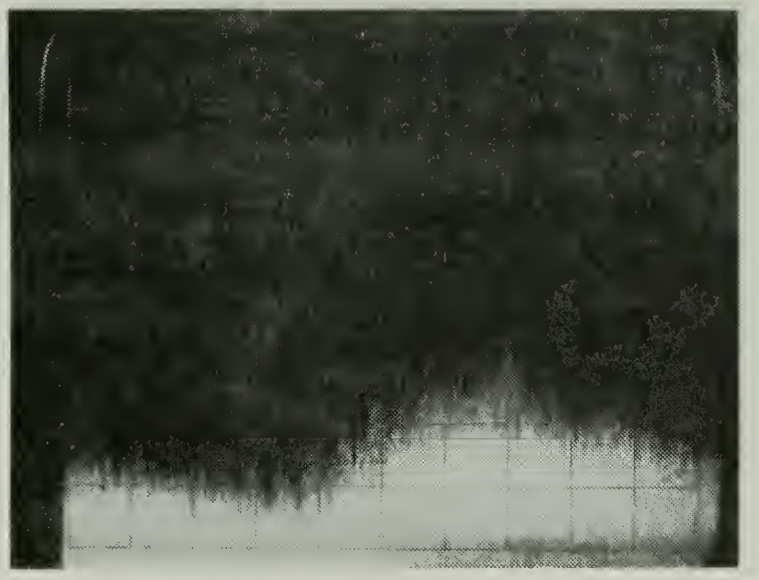

Figure 22.

Local oscillator contaminating signal 4 minutes after laser was re-energized: Center frequency 40 MHz, Spectrum analyzer dispersion 2 MHz/Div, Right side of figure is low frequency.

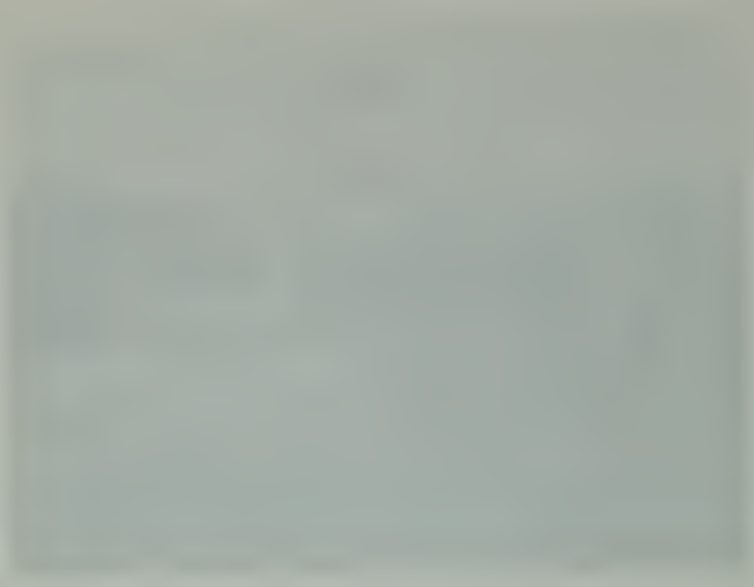

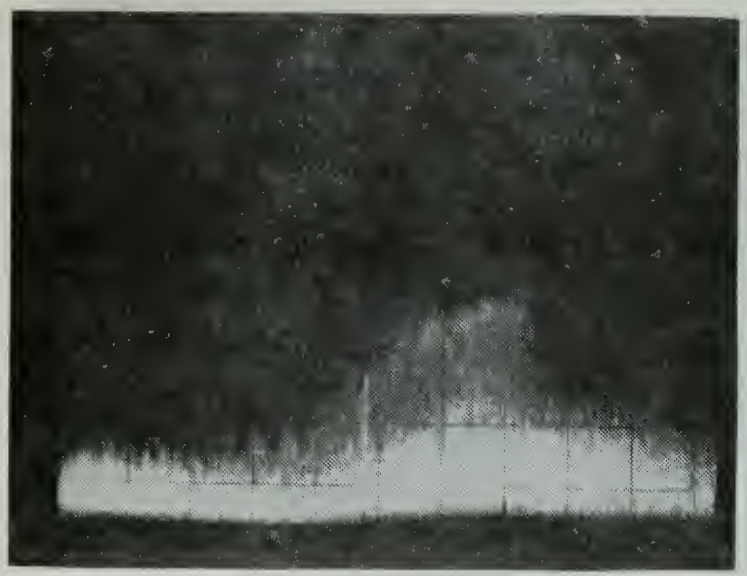

Figure 23.

Local oscillator contaminating signal 5 minutes after laser was re-energized. All measurement parameters are as in Figure 22.

Figure 24.

Local oscillator contaminating signal 7 minutes after laser was re-energized. All measurement parameters are as in Figure 22.

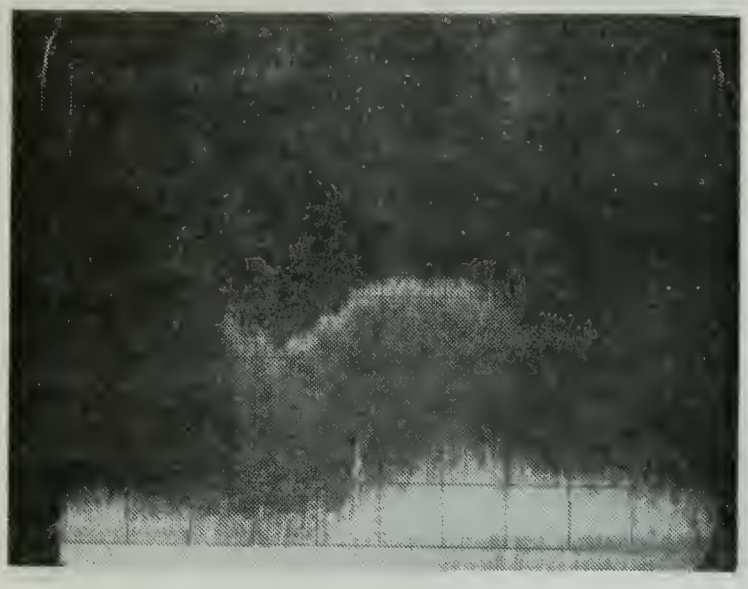

Figure 25.

Local oscillator contaminating signal 2 minutes after laser was re-energized. All measurement parameters are as in Figure 22.

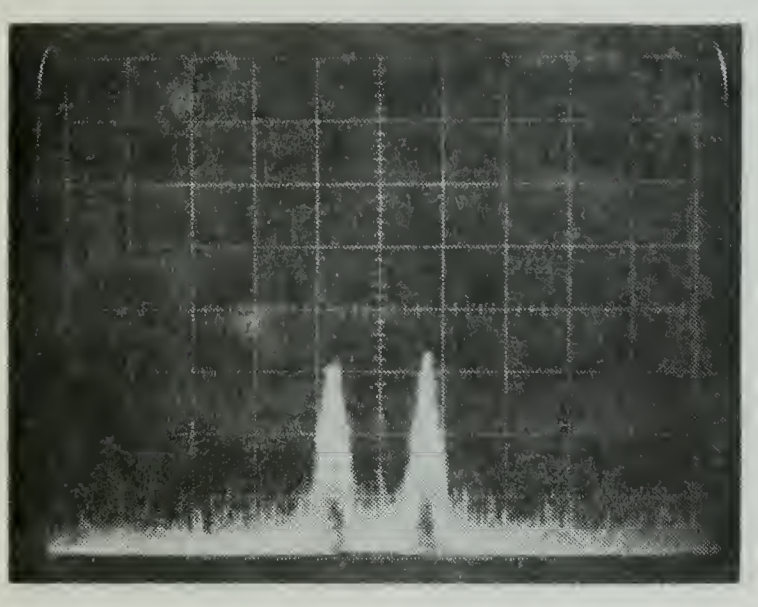

Figure 26.

Zero range offset. The range offset is visible via the local oscillator contaminating signal: Center frequency 30 MHz, Spectrum analyzer dispersion 50 kHz/Div.

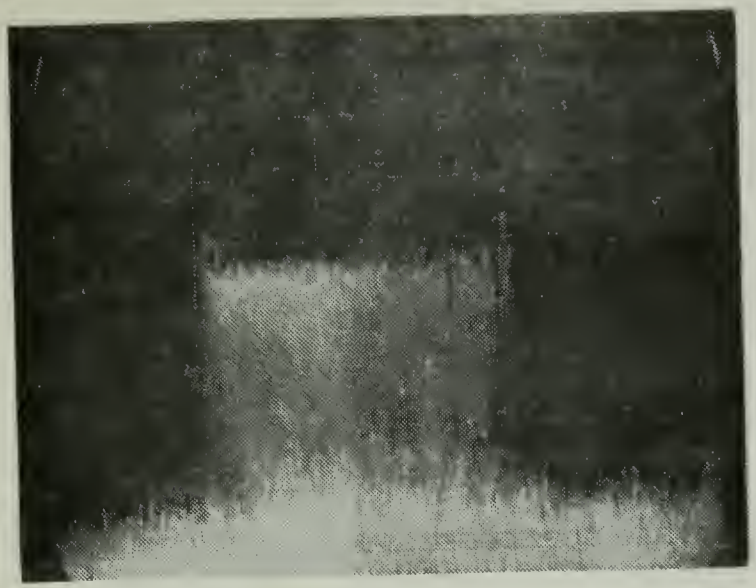

Figure 27.

Heterodyne detected signal prior to electronic processing: Center frequency 40 MHz, Spectrum analyzer dispersion 2 MHz/Div.

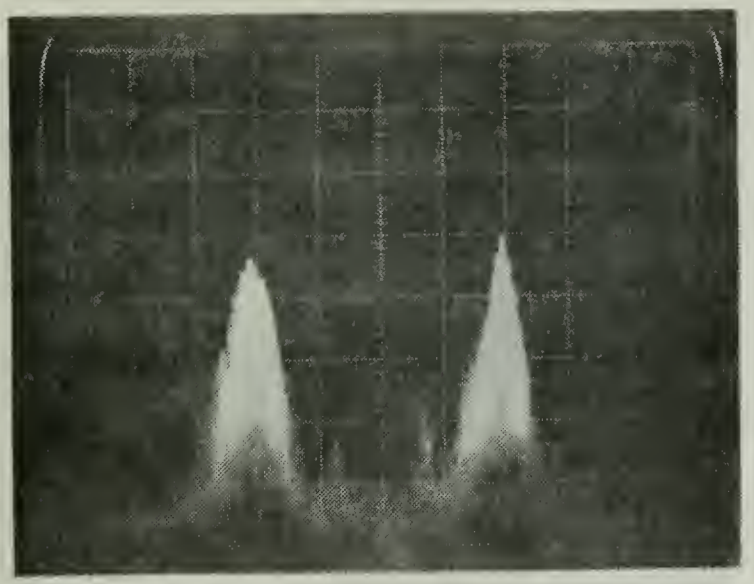

Figure 28.

Processed signal of a stationary target at 305 yards. 40 db of attenuation is inserted prior to the spectrum analyzer. Note the visible zero range offset. Center frequency 30 Mhz, Spectrum Analyzer dispersion 50 kHz/Div.

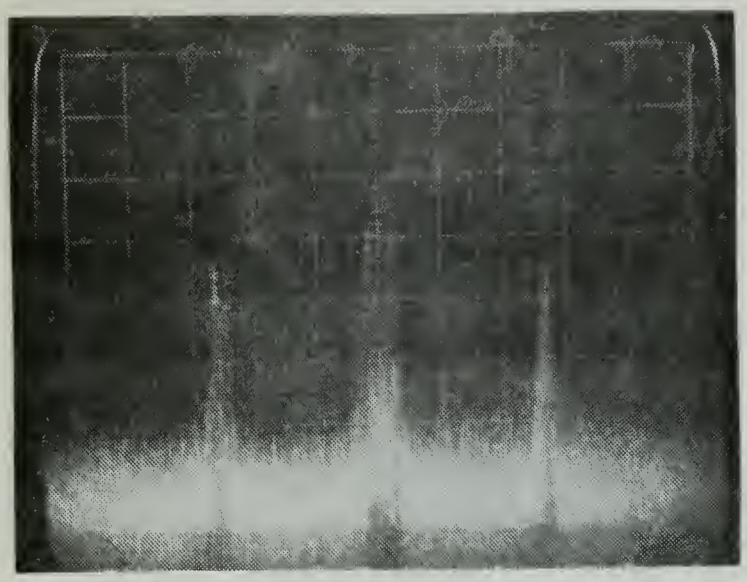

Figure 29.

Processed signal from a stationary target at 2400 yards. No attenuation inserted. Note that the zero range offset is clearly visible: Center frequency 30 MHz, Spectrum Analyzer dispersion 200 kHz/Div.

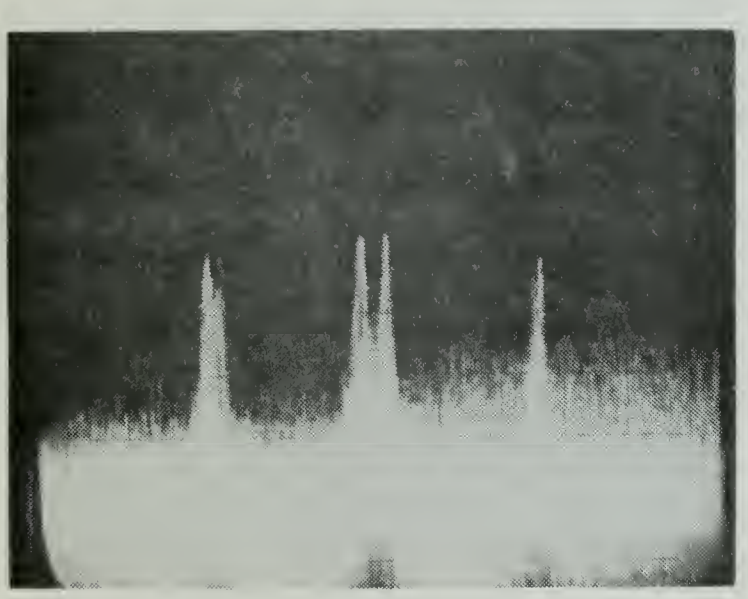

Figure 30.

Processed signal from a stationary target at 2400 yards. All measurement information is the same as in Figure 29.

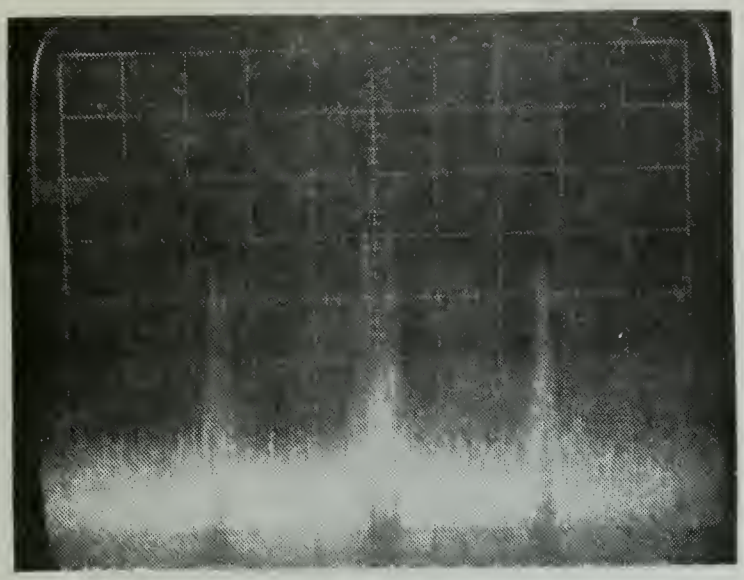

Figure 29.

Processed signal from a stationary target at 2400 yards. No attenuation inserted. Note that the zero range offset is clearly visible: Center frequency 30 MHz, Spectrum Analyzer dispersion 200 kHz/Div.

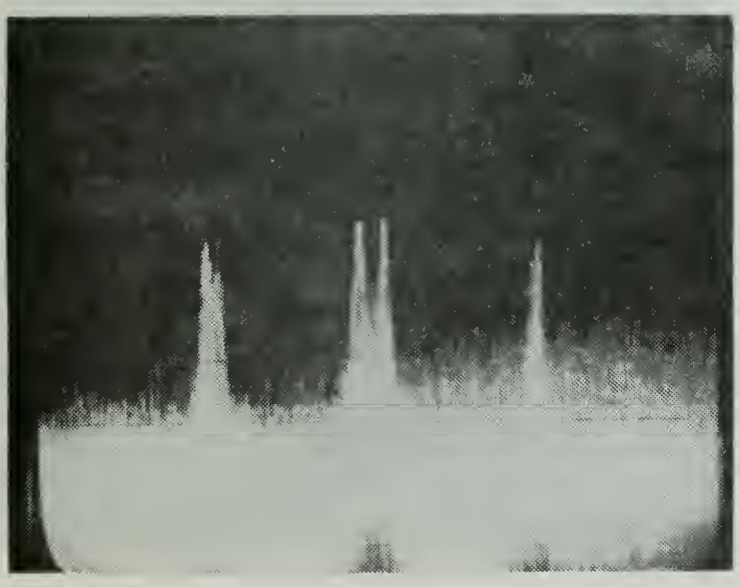

Figure 30.

Processed signal from a stationary target at 2400 yards. All measurement information is the same as in Figure 29.

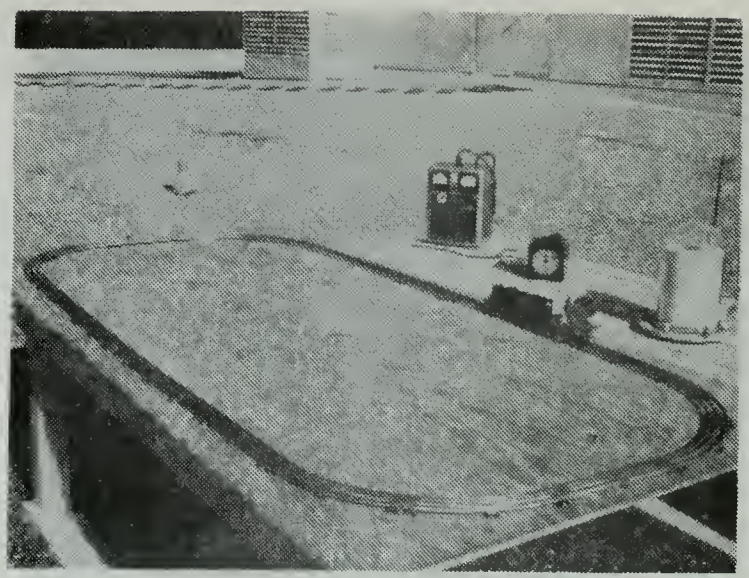

Figure 31.

Target velocity generation apparatus.

Figure 32.

Target retro-reflector.

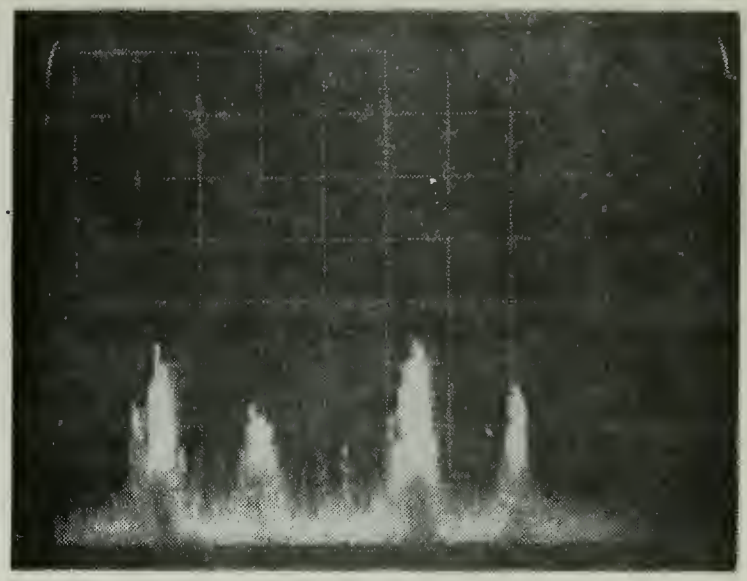

Figure 33.

Simultaneous range and velocity information from a moving target at 305 yards: Center frequency 30 MHz, Spectrum analyzer dispersion 50 kHz/Div.

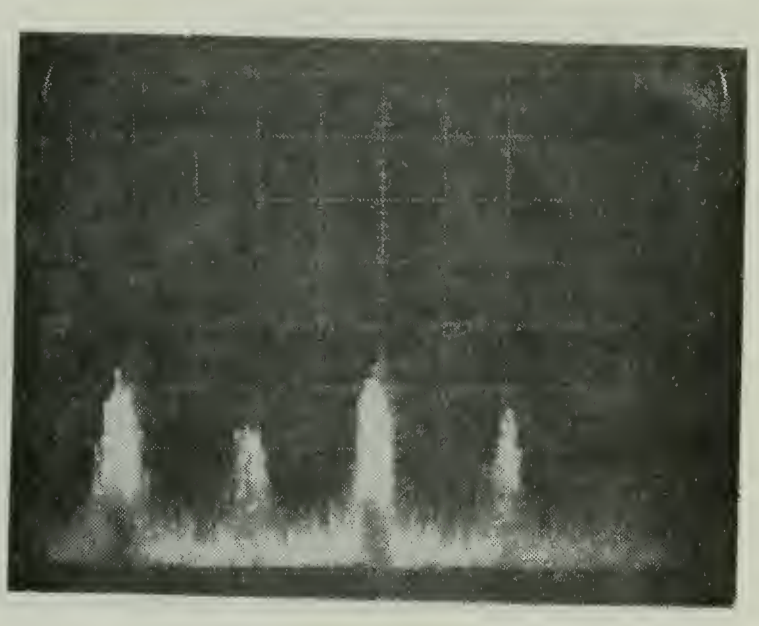

Figure 34.

Simultaneous range and velocity information from a moving target at 305 yards. Note the presence of a stationary target return. All measurement data are the same as for Figure 33.

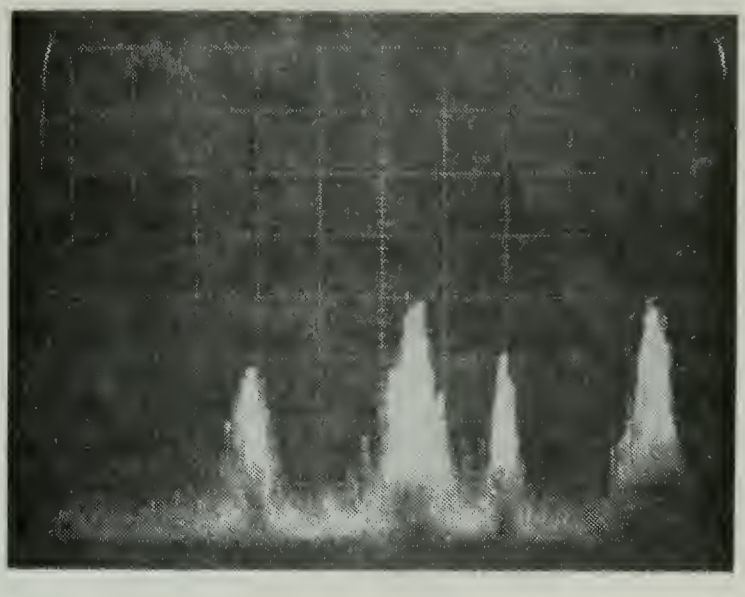

Figure 35.

Simultaneous range and velocity information from a moving target at 305 yards: Measurement data are the same as for Figure 33.

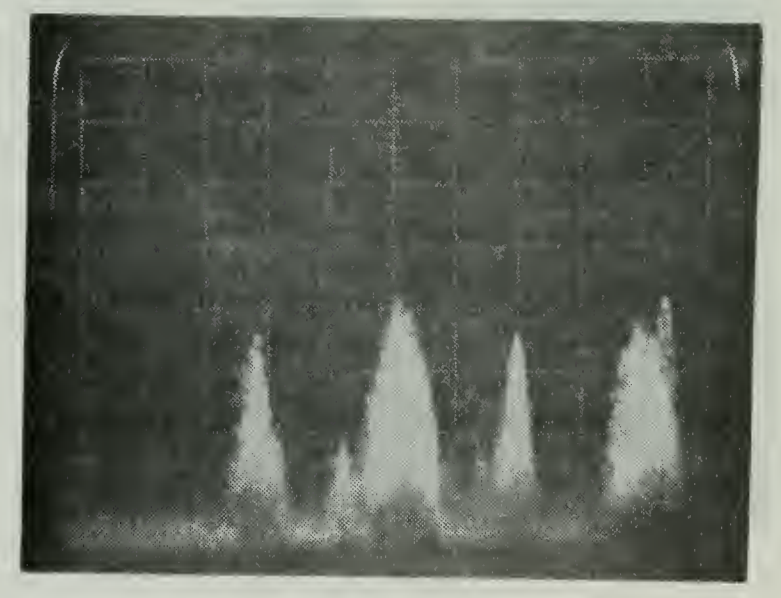

Figure 36.

Simultaneous range and velocity information from a moving target at 305 yards: Measurement data are the same as for Figure 33.

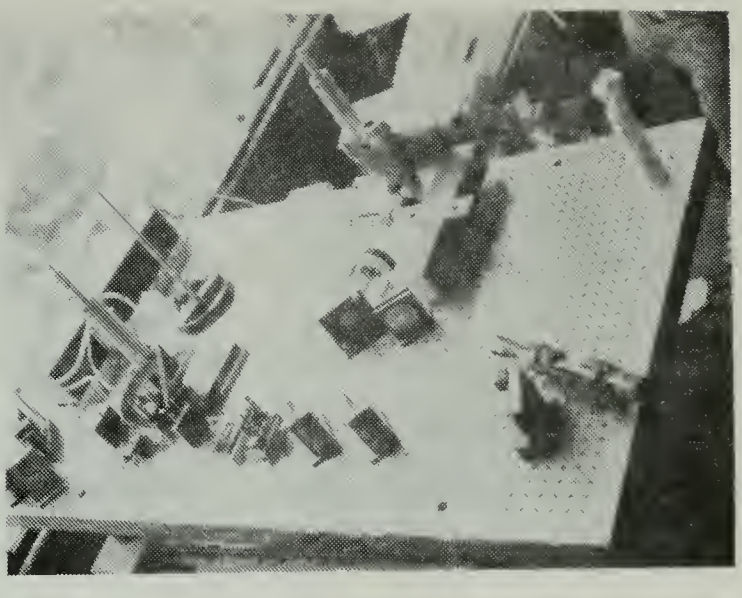

Figure 37.

Photograph of optical components utilized in the first optical configuration (Figure 14).

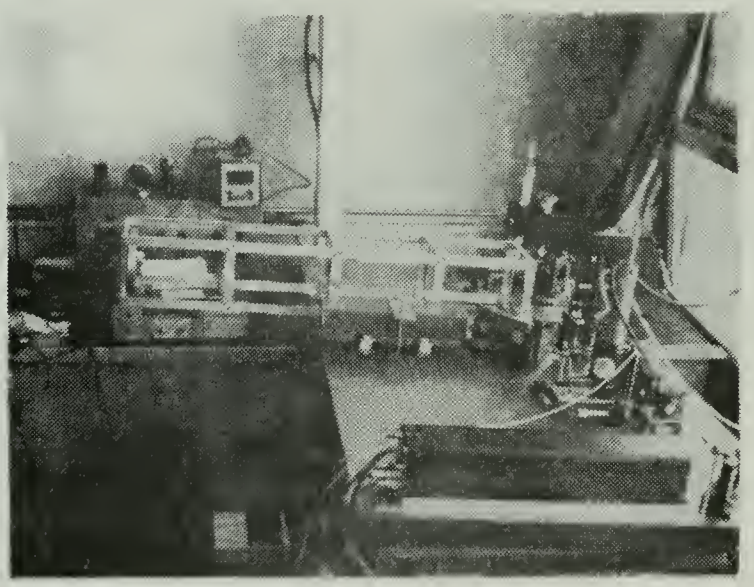

Figure 38.

Photograph of the optical components utilized in the second optical configuration (Figure 15).

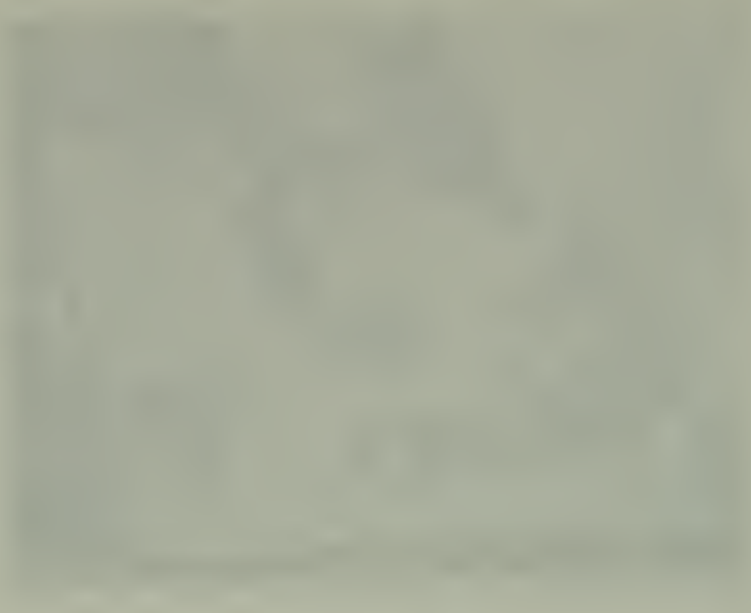

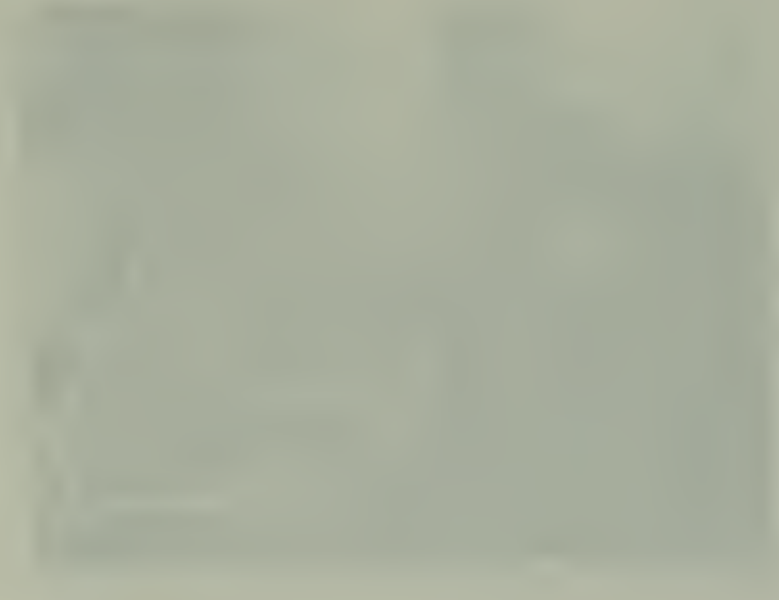

APPENDIX A

EQUIPMENT LIST

Unidek Optical Table, Quarter inch tapped holes drilled on a one inch grid spacing.

CO_2 Laser, Honeywell Model 3000.

Modulator-Driver, Isomet Model DE-IR-10/S.

Acousto-Optic Modulator, Isomet Model DE-IR-10.

Spectrum Analyzer, Tektronix, Inc., Model 491.

Oscilloscope, Tektronix, Inc., Model 546.

Detector Bias and Pre-amplifier, Mfg. by NELC Code 2500. (23 db Amplification with a 3 db Noise Figure)

Signal Amplifier (2-100 MHz), Miteq Model AV-1A-3078-3.

Wideband Amplifier, Two Cascaded Hewlett Packard Model 461A.

Function Generator, Wavetek Model 134.

Signal Generator, Hewlett Packard Model 606A.

Analog Optical Power Meter, Coherent Radiation Model 201.

Digital Optical Power Meter, Jordon Model PM-550.

Balanced Modulators (Mixers - .2-500 MHz), Relcom Model M1.

DC Power Supplies, Hewlett Packard Model 6216A.

Beamsplitters, Laser Optics 2 Inch Diameter Germanium Splitters with Anti-reflective Coating on the Exit Surface.

Detector Focus Lens, Laser Optics 2 Inch Diameter Germanium Lens with Anti-reflective Coatings.

Beam Elevators, Spectra-Physics Model 340.

Band Pass Filter (BPF), 65-80 MHz Butterworth Band Pass Filter Designed and Constructed by the Author.

High Pass Filter (HPF), Simple Parallel LC filter with a Center Frequency of 40 MHz. Constructed by the Author.

Infrared Detector, Raytheon Model IR-101, Sensitive area approximately 10 Mils diameter.

Infrared Detector, Rockwell International Number 5-128-4, Sensitive area approximately 7 Mils diameter.

Infrared Detector, Rockwell International Number 7-229A, Sensitive area approximately 7 Mils diameter.

Infrared Detector, Aerojet General Corp. Sample number unknown. Sensitive area approximately 5 Mils diameter.

Encapsulated Liquid Crystal Paper, Edmund Scientific Co. Stock Number 500224.

BIBLIOGRAPHY

1. Oliver, B. M., "Signal to Noise Ratios in Photoelectric Mixing," IRE Proceeding, v. 49, p. 1969-1961, December 1961.

2. Peyton, B. J., and others, "High-Sensitivity Receiver for Infrared Laser Communications," IEEE Journal of Quantum Electronics, v. QE-8, p. 252-263, February 1972.

3. Ross, M., Laser Receivers, Wiley, 1966.

4. Pratt, W. K., Laser Communications Systems, Wiley, 1969.

5. Peyton, B., and others, "Coherent Infrared Receivers for Laser Communications and Radar," Internal paper of AIL, a division of Cutter-Hammer Melville, Long Island, New York, 1973.

6. Arams, F. R., Sard, E. W., and Peyton, B. J., "5.2 - Infrared 10.6 - Micron Heterodyne Detection with Gigahertz IF Capacility," IEEE Journal of Quantum Electronics, v. QE-3, p. 484-492, November 1967.

7. Chance, T. H., FM-CW Laser Radar at 10.6 Microns, Electrical Engineer Thesis, Naval Postgraduate School, Monterey, California, 1974.

8. Jamieson, J. A. and others, Infrared Physics and Engineering, McGraw-Hill, 1963.

9. Hudson, R. D., Infrared System Engineering, Wiley, 1969.

10. Soze, S. M., Physics of Semiconductor Devices, Wiley, 1969.

11. Melchior, H., Fisher, M. B., and Arams, F. R., "Photodetectors for Optical Communications Systems," Proceedings of the IEEE, v. 58, p. 1466-1485, October 1970.

12. Holmquist, K. E., Thin-Film $Pb_{0.9}Sn_{0.1}Se$ Photoconductive Infrared Detectors: Photoconductivity Measurements, Masters Thesis, Naval Postgraduate School, Monterey, California, 1972.

13. Santa Barbara Research Center Contract DAAK02-73-C-0147, High Density Lead Tin Telluride Detector Array, by F. J. Renda, February 1974.

14. Raytheon Report SM-313, Second Interim Report Development of Lead-Tin Telluride Detectors, by Debye, P. P., Kennedy, C. A., and Linden, K. J., January 1972.

15. Burke, C., and Koehler, T., "10.6 μm Detection at 170°K," paper presented at Sixth DOD Laser Conference, Colorado Springs, Colorado, 26-28 March 1974.

16. DeLangue, O. E., "Optical Heterodyne Detection," IEEE Spectrum, v. 5, p. 77-85, October 1968.

17. Skolnik, M. I., Radar Handbook, McGraw-Hill, 1970.

18. Hoisington, D. B., "Multiple-Target CW-FM Radar," paper presented at 6th Asilomar Conference on Circuits and Systems, Pacific Grove, California, November 1972.

19. Hymans, A. J., and Lait, J., "Analysis of a Frequency-Modulated Continuous-Wave Ranging System," Proceedings IEE (British), Paper No. 3264E, p. 365-372, July 1970.

20. Kay, L., "A Comparison between Pulse and Frequency-Modulation Echo-Ranging Systems," Journal Brit. IRE, p. 105-113, February 1959.

21. Kaminow, I. P., and Turner, E. H., "Electrooptic Light Modulators," Proceedings of the IEEE, v. 54, p. 1374-1389, October 1966.

22. Chen, F. S., "Modulators for Optical Communications," Proceedings of the IEEE, v. 58, October 1970.

23. Born, M., and Wolf, E., Principles of Optics, 4th ed., Pergamon Press, 1970.

24. Gordon, E. I., "A Review of Acoustooptic Deflection and Modulation Device," Proceedings of the IEEE, v. 54, p. 1391-1401, October 1966.

25. Adler, R., "Interaction between Light and Sound," IEEE Spectrum, v. 4, p. 42-54, May 1967.

26. Dixon, R. W., and Gordon, E. I., "Acoustic Light Modulators Using Optical Heterodyne Mixing," The Bell System Technical Journal, v. 46, p. 367-389, February 1967.

27. Yariv, A., Introduction to Optical Electronics, Holt, Rinehart, and Winston, 1971.

28. Davis, J. I., "Considerations of Atmospheric Turbulence in Laser System Design," Applied Optics, v. 5, p. 139-147, January 1966.

29. Tatarski, V. I., Wave Propagation in a Turbulent Medium, McGraw-Hill, 1961.

30. Fried, D. L., "Optical Resolution through a Randomly Inhomogeneous Medium for Very Long and Very Short Exposures," Journal of Optical Society of America, v. 56, p. 1372-1378, October 1966.

31. Fried, D. L., "Optical Heterodyne Detection of an Atmospherically Distorted Signal Wavefront," Proceedings of the IEEE, v. 55, p. 57-67, January 1967.

32. Gilmartin, T. J., and Holtz, J. Z., "Focused Beam and Atmospheric Coherence Measurements at 10.6 μm and 0.63 μm," Applied Optics, v. 13, p. 1906-1912, August 1974.

33. ITT Federal Laboratories, Measurement of the Degree of Coherence for Laser Light Traversing Fogs, by J. M. Grant and H. Y. Ageno, 9 October 1964.

34. Corcoran, V. J., "Directional Characteristics in Optical Heterodyne Detection Processes," Journal of Applied Physics, v. 36, p. 1819-1825, June 1965.

35. Siegman, A. E., "The Antenna Properties of Optical Heterodyne Receivers," Proceedings of the IEEE, v. 54, p. 1350-1356, October 1966.

36. Read, W. S., and Turner, R. G., "Tracking Heterodyne Detection," Applied Optics, v. 4, p. 1570-1573, December, 1965.

37. Rockwell International Science Center Report SC560-IM/DD, 10.6 Micron Photodiodes, by A. S. Joseph, p. 10, 27 September 1973.

INITIAL DISTRIBUTION LIST

		No. Copies
1.	Defense Documentation Center Cameron Station Alexandria, Virginia 22314	2
2.	Library, Code 0212 Naval Postgraduate School Monterey, California 93940	2
3.	Department Chairman, Code 52 Department of Electrical Engineering Naval Postgraduate School Monterey, California 93940	2
4.	Assoc. Professor T. N. Tao, Code 52 Tv Department of Electrical Engineering Naval Postgraduate School Monterey, California 93940	1
5.	Asst. Professor J. P. Powers, Code 52 Po Department of Electrical Engineering Naval Postgraduate School Monterey, California 93940	1
6.	Assoc. Professor G. L. Sackman, Code 52 Sa Department of Electrical Engineering Naval Postgraduate School Monterey, California 93940	1
7.	Naval Electronics Laboratory Center Code 2500 271 Catalina Boulevard San Diego, California 92152	2
8.	LT Thomas H. Chance U.S. Naval Destroyer School, Class 6 Jan 75 Newport, Rhode Island 02840	1
9.	LT Maurice F. Fraunfelder 1302 Putnam Avenue Janesville, Wisconsin 53545	1

157375

Thesis
F7857 Fraunfelder
c.1
A heterodyne detection
FM-CW laser radar using
10.6 μ source.